

RESEARCH ARTICLE

10.1002/2016GC006336

Water-rich and volatile-undersaturated magmas at Hekla volcano, Iceland

Gregor Lucic¹, Anne-Sophie Berg¹, and John Stix¹¹Department of Earth and Planetary Sciences and GEOTOP, McGill University, Montreal, Quebec, Canada

Key Points:

- Positive correlation among repose interval, magmatic evolution, and volatile content of magmas
- Explosive eruptions of H₂O-rich and CO₂-poor magmas that may be volatile undersaturated
- Generation and storage of silicic magmas within Iceland's middle and lower crust

Supporting Information:

- Figures S1–S2
- Tables S1–S8

Correspondence to:

G. Lucic,
gregor.lucic@mail.mcgill.ca

Citation:

Lucic, G., A.-S. Berg, and J. Stix (2016), Water-rich and volatile-undersaturated magmas at Hekla volcano, Iceland, *Geochem. Geophys. Geosyst.*, *17*, 3111–3130, doi:10.1002/2016GC006336.

Received 1 MAR 2016

Accepted 12 JUL 2016

Accepted article online 14 JUL 2016

Published online 8 AUG 2016

Corrected 15 SEPT 2016

This article was corrected on 15 SEPT 2016. See the end of the full text for details.

Abstract Olivine-hosted melt inclusions from four eruptions at Hekla volcano in Iceland were analyzed for their dissolved H₂O, CO₂, S, and Cl contents. A positive correlation among the repose interval, magmatic evolution, and volatile contents of magmas is revealed. H₂O is the dominant volatile species; it behaves as an incompatible component, increasing in concentration over time as a result of fractional crystallization in the magma. The full suite of H₂O contents ranges from a low of 0.80 wt % in basaltic andesites to a maximum of 5.67 wt % in rhyolites. Decreasing H₂O/K₂O at fixed major element compositions suggests that syneruptive degassing reduces H₂O contents significantly. Hekla magmas are CO₂ poor, with very low concentrations present only in the most evolved compositions (~20–30 ppm or less). The decrease in S content from basaltic andesite to rhyolite demonstrates that sulfide saturation is attained when the melt composition reaches basaltic andesite, resulting in the precipitation of pyrrhotite. Low CO₂/Nb ratios suggest that vapor saturation is most likely reached during an early period of cooling and solidification in the crust. Fresh injections of mafic magma interact with previously solidified intrusives, producing new melts that are volatile undersaturated. Vapor saturation pressures obtained using the most volatile-rich melt inclusions suggest the presence of a magma chamber at a minimum depth of ~7 km. This is in agreement with geophysical observations from recent small-volume eruptions, but given the possibility of volatile-undersaturated melts, some of the magmas may reside at greater depths.

1. Introduction

The generation and evolution of water-rich silicic magmas at volcanic centers in Iceland have been a topic of great interest and debate [Bindeman *et al.*, 2012; Hards *et al.*, 2000; Jónasson, 2007; Kuritani *et al.*, 2011; Lacasse *et al.*, 2007; Martin and Sigmarsson, 2010]. Spreading systems are commonly associated with H₂O-poor mafic magmas, yet in Iceland, there are voluminous eruptions of H₂O-rich silicic magmas. The origin of these magmas is thought to be a function of crustal assimilation at various storage depths, crystal fractionation, and long residence times within the thickened Icelandic crust [Schattel *et al.*, 2014]. Detailed tephrochronological and geochemical studies at Hekla volcano, one of Iceland's most active and productive volcanic centers, have revealed that the volume of erupted material, explosivity, composition of the first erupted material and length of the eruption are directly related to the duration of the preceding repose period [Thorarinsson, 1967; Larsen *et al.*, 1999]. In other words, the longer the repose period, the more evolved, explosive, and voluminous the eruption. This is a key finding and makes this volcano an ideal natural laboratory for the study of volatile contents in both mafic and silicic magmas.

In this report, we present a detailed volatile study of four eruptions from Hekla volcano. Our aim is to address the following key questions. (1) How do volatile contents compare and contrast among large, medium and small eruptions of different compositions? (2) Are the magmas volatile saturated or unsaturated prior to eruption? (3) Are large and small eruptions sourced from the same magma chamber, or is there any indication of multiple reservoirs? (4) What can H₂O-CO₂ relationships tell us about the storage depths and evolution of silicic versus mafic magmas at Hekla and in Iceland more generally?

2. Hekla Volcano

Hekla's first historic eruption was recorded in 1104 A.D.; since that event it has erupted at least 18 times [Thorarinsson, 1967; Thorarinsson and Sigvaldason, 1972; Gronvold *et al.*, 1983; Gudmundsson *et al.*, 1992]. In

addition to these historic events, stratigraphic records reveal that Hekla's largest and most voluminous eruptions occurred in the Holocene between 1104 A.D. and >7000 B.P. [Larsen and Thorarinsson, 1977]. Its most recent eruption was small and from the southwest flank in February 2000.

2.1. Evolution of Magmas

Eruptive products at Hekla vary from rhyolite to basalt. This range is thought to be a product of magmatic evolution at different stages [Sigmarsson *et al.*, 1992; Sverrisdottir, 2007; Chekol *et al.*, 2011; Portnyagin *et al.*, 2012]. (1) Initial basaltic melts rise through the crust where they evolve to basaltic andesites through fractional crystallization. (2) If these melts reside in the tholeiitic host rocks for a sufficient length of time, they evolve to dacites through a combination of fractional crystallization and crustal assimilation. If the residence time is sufficiently long, they can evolve to rhyolites. (3) Injections of basaltic andesites into these evolved chambers may produce hybrid mixtures of magma and contribute to the development of compositionally stratified magma chambers. These injections also may force the chamber into disequilibrium and trigger an eruption. (4) Less evolved compositions spend less time in the crust and may ascend with little or no assimilation and smaller amounts of fractional crystallization. The extent to which hydrothermally altered crustal rocks are assimilated is a topic of debate and discussed below.

2.2. Magma Storage

While the overall model of magmatic evolution at Hekla appears to be generally established, there is much discussion regarding the depth and size of magma chambers beneath the volcano. Melt inclusion data on the saturation pressure of H₂O provide an estimate of the minimum depth of storage at 9 km depth for the 1916 and 2000 basaltic eruptions [Moune *et al.*, 2007] and 5–6 km for the H3 and H4 silicic eruptions [Portnyagin *et al.*, 2012]. A review of geophysical estimates presented below suggest the presence of a magma reservoir in the shallow to mid-crustal depths (4–7 km) along with a secondary reservoir at much greater depths (~20 km).

After the 1980–1981 eruption, inflationary signals suggested the presence of a magma chamber 5.5×10^7 m³ in volume, centered at a depth of 7.7 km [Kjartansson and Gronvold, 1983]. Dilatational strain during the 1991 eruption suggested that magma was being erupted through a dyke, sourced from a magma chamber at 6.5 km depth with a radius of 2.5 km [Linde *et al.*, 1993]. The propagation of the dyke initiated at 4 km depth, which could represent the roof of the magma chamber. The deflation signal during the 1991 eruption was centered at 9 ± 6.5 km deep, with a volume of $1.45 \pm 0.60 \times 10^{11}$ m³ and modeled as a spherical chamber with a radius of 3.5 km [Sigmundsson *et al.*, 1992]. Ofeigsson *et al.* [2011] used InSAR data to identify two sources associated with the 2000 event. In the period leading up to the eruption (1993–2000), they detected an inflation signal that shared a common source with the co-eruptive deflation during the event. They placed the first source at a depth of 14–18 km with a volume of 4×10^7 – 8×10^7 m³. The second source produced a local inflation signal thought to be associated with the opening of the dyke. This signal had a source at 5.6 km depth, with an estimated volume of 5×10^6 – 6×10^6 m³. Geirsson *et al.* [2012] used GPS data to model a horizontal ellipsoid magma chamber at a depth of 24 ± 4 km depth, a spherical magma chamber at 24 ± 5 km depth, or a vertical pipe-shaped chamber stretching between 10 and 21 km. In either case, the bulk of magma accumulation was interpreted to occur at deep crustal levels close to the Moho, which is situated somewhere between 20 and 29 km depth beneath Hekla [Allen *et al.*, 2002]. Sturkell *et al.* [2013] presented a review of deformational data at Hekla and concluded that the main reservoir is centered at ~10 km depth. Soosalu and Einarsson [2004] found no seismic evidence of any magma chamber in the 5–8 km depth range. Their *S* wave attenuation data indicate a reservoir either shallower than 4 km or deeper than 14 km. However, the lack of hydrothermal activity argues against a reservoir shallower than 4 km [Ilyinskaya *et al.*, 2015].

Given this large range in depth estimates obtained from geochemistry and geophysics, it remains difficult to establish a robust model for the plumbing network beneath Hekla. Modern-day monitoring covers a period in the volcano's history characterized by small eruptions of mafic compositions. In particular, we lack geophysical observations and direct measurements of volatile contents for the full range of eruptive styles and compositions from basalt to rhyolite. This is especially significant if we consider that the magmatic network was possibly reconfigured following the 1947 eruption [Sturkell *et al.*, 2013].

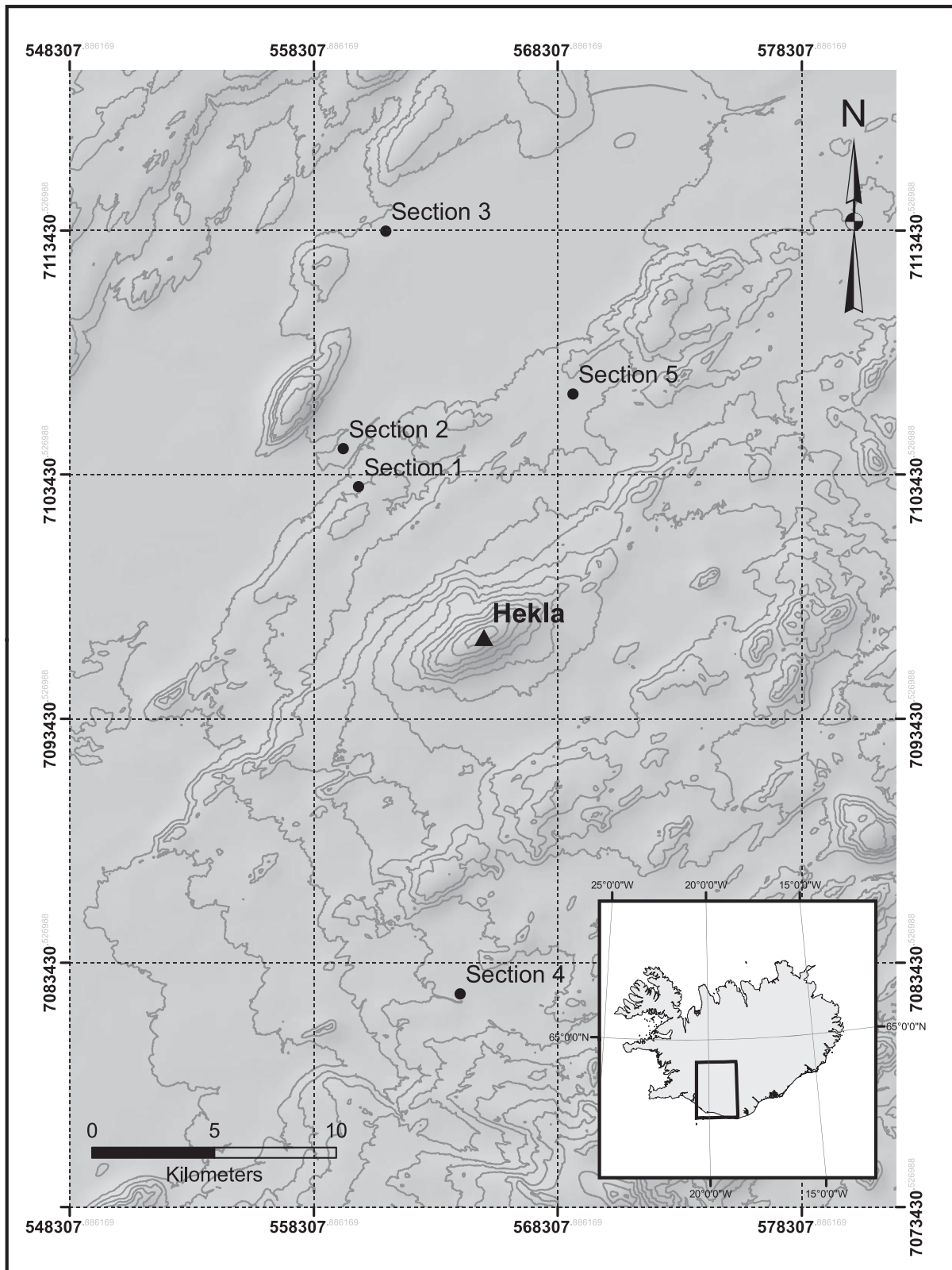


Figure 1. Topographic map of Hekla volcano and surrounding area. The summit of the volcano (triangle) and sampling localities (dots) are marked for reference. The map coordinates represent the WGS1984 datum, UTM zone 27°N.

3. Sampling and Analytical Methods

3.1. Fieldwork

Deposits of four eruptions were sampled for volatile analysis in olivine-hosted melt inclusions. They are Holocene 3 or H3 (2880 years B.P., ¹⁴C age from *Dugmore et al.* [1995]), 1104, 1845, and 1991. These eruptions were chosen to represent a range in repose periods, compositions and volumes of erupted material. Samples were collected from exposures at five sections located at various distances and directions from Hekla (Figure 1).

The deposits of Hekla's largest and most voluminous eruption, H3, feature compositional zonation from 67.8 wt % SiO₂ (whole rock on an anhydrous basis) at the base to 56.2 wt % at the top [*Sverrisdottir, 2007*]. The total volume of erupted material (lava and tephra) is estimated at 2.2 km³ DRE [*Sverrisdottir, 2007*]. The andesite end-member was not sampled in this study, but it has been examined by others [*Sverrisdottir, 2007; Portnyagin et al., 2012*]. The most striking feature of the deposit, best illustrated at section 1, is a change in color from white pumice fragments at the base of the deposit to reddish or pinkish pumice fragments at the top (Figures 2 and 3). A third break can be seen at section 2, where the top 15 cm of the deposit are characterized by the presence of darker pumice fragments. Based on these differences, we collected samples from three horizons: HK2013-H3-A (H3 base), HK2013-H3-B (H3 light top), and HK2011-H3-C (H3 dark top) (Figures 2 and 3).

In many respects, the 1104 deposit appears to be a smaller version of H3 (0.5 km³ DRE from *Sverrisdottir* [2007]). Gradual changes in pumice color at ~20 cm, changes in grain size, and the presence of a distinctive grey top suggest a zoned deposit. Whole rock data reveal that 1104 is in fact a rhyolite [*Thorarinsson, 1967*], recognized in Icelandic tephrochronology by its distinctive white color. At the sampled locality, the deposit is characterized by two normally graded pumice layers, the first 30 cm in thickness, overlain by a second 15 cm in thickness. Many of the pumices in the upper layer have grey banding, a feature that contributes to an overall change in color near the top of the deposit. The uppermost 5 cm of the deposit are marked by a distinct layer of grey pumice fragments interbedded with ash. Based on these distinctions, our sampling at section 3 was divided into HK2013-1104-A (1104 base), HK2013-1104-B (1104 light top), and HK2013-1104-C (1104 dark top) (Figures 2 and 3).

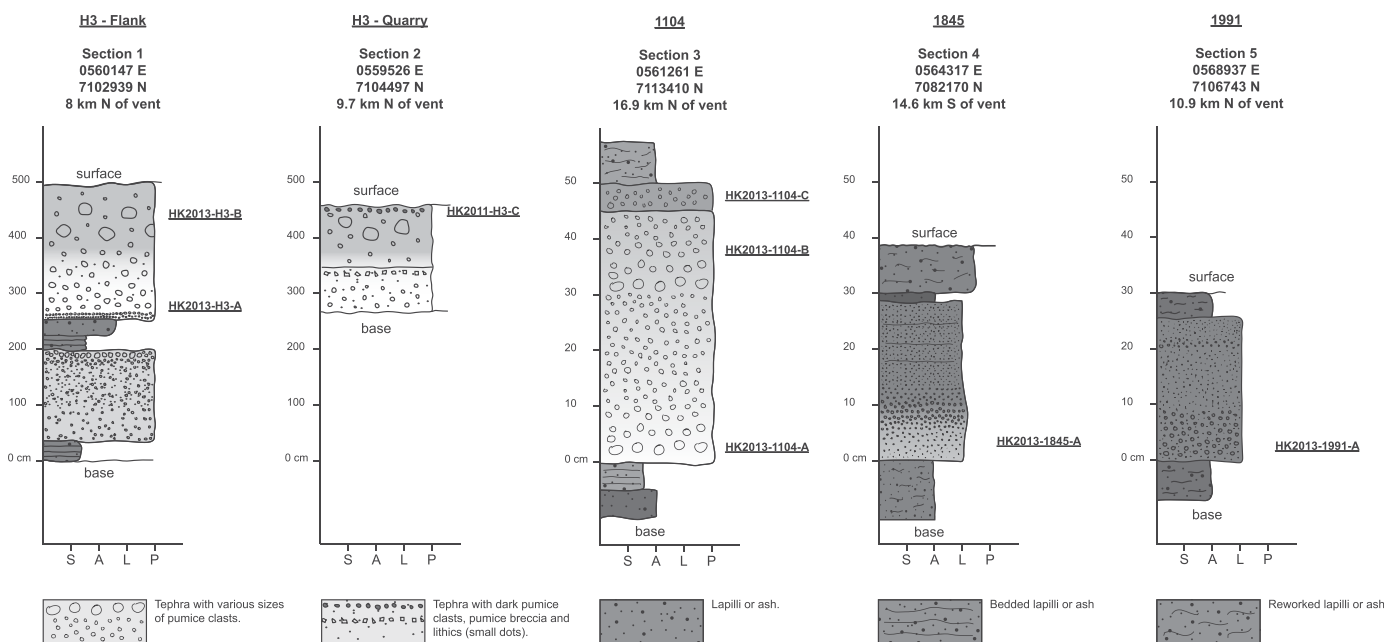


Figure 2. Stratigraphic sections of sampling localities for the H3, 1104, 1845, and 1991 eruptions. Each sampling horizon is marked with a unique ID that represents the name of the volcano (HK), sampling year (e.g., 2013), eruption name (e.g., 1104), and relative horizon (A = base, B = light top, and C = dark top). Datum is WGS1984, UTM zone 27°N. For locations from Hekla's summit, see Figure 1. Grain sizes are listed as S for soil, A for ash, L for lapilli, and P for pumice.

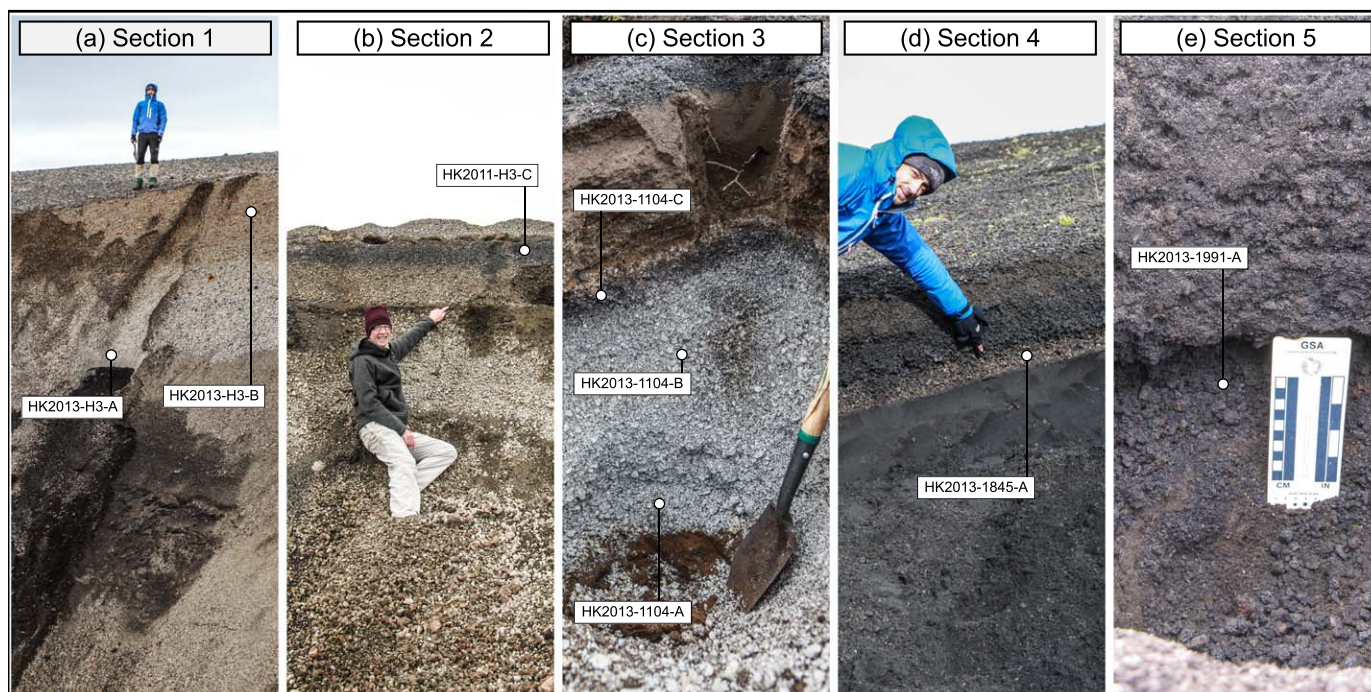


Figure 3. Field photographs of the sampling sections marked with sampling horizons. (a) At Section 1, G.L. is standing on top of H3 light top. Note the change in color from white pumice fragments at the base to pink pumice fragments at the top. (b) At Section 2, J.S. points to a thin, ashy soil horizon, possibly a discontinuity. Note the dark horizon of pumice fragments, representative of H3 dark top. (c) At Section 3, we observe a distinct color change between the bulk of the 1104 deposit and its darker top. (d) At Section 4, G.L. points at a change in color from light pumice fragments to dark pumice fragments within the 1845 deposit. (e) At Section 5, tephra from the 1991 eruption is exposed by removing 30–40 cm of reworked material from the surface.

The 1845 deposit was sampled at section 4 (Figures 2 and 3). Similar to H3, this deposit is zoned but smaller in volume than H3 and slightly larger than 1104 (0.63 km³ DRE from *Sverrisdottir* [2007]). The deposit is characterized by fine lapilli at the base that grade upward into coarse lapilli. The increase in grain size is accompanied by an upward change to a darker color at 10 cm from the base which is associated with a change in whole rock composition from andesite to basaltic andesite [*Thorarinnsson*, 1967]. Samples from the 1845 package were restricted to a single horizon from the bottom 10 cm and referred to as HK2013-1845-A (or 1845).

The least evolved unit is that of the 1991 eruption, sampled on the northern flank of the volcano at section 5 (Figures 2 and 3). The deposit at this locality is 25 cm thick, reflecting the small volume of the eruption (0.15 km³ DRE from *Sverrisdottir* [2007]). There is no indication of zonation in whole rock compositions from base to top, but there are distinct changes in grain size suggestive of two main eruptive pulses. This is in agreement with observations of tephra fall during the eruption [*Gudmundsson et al.*, 1992]. Whole rock compositions of the tephra and lavas plot within the basaltic andesite field (54 wt % SiO₂) [*Gudmundsson et al.*, 1992; *Chekol et al.* 2011]. Samples from the 1991 eruption were collected at the base of the deposit and labeled HK2013-1991-A (or 1991).

3.2. FTIR Analysis

Melt inclusions were analyzed using a Bruker Tensor 27 infrared spectrometer paired with a Bruker Hyperion 2000 microscope. Analyses were conducted with a 15X objective lens in transmission mode using a spectral resolution of 4 cm⁻¹ and 256 scans for both background and sample measurements. The optical aperture was adjusted to enable three separate measurements of the same melt inclusion. With larger melt inclusions (~150 μm), it was possible to separate these points by 10 μm, but with smaller inclusions it was only possible to move the stage by 1–3 μm. In both cases, there was overlap between the sampling areas. Testing on in-house glass standards produced reproducible spectra down to an aperture diameter of 20 μm.

Peak heights for the 5200 cm⁻¹ (H₂O_m), 4500 cm⁻¹ (OH⁻), and 1630 cm⁻¹ (H₂O_m) peaks were obtained using baselines following *Newman et al.* [1986], while the peak heights for the 3450 cm⁻¹ (H₂O_m + OH⁻)

Table 1. FTIR Extinction Coefficients

Wave number (cm ⁻¹) Volatile species	E ₅₂₀₀ H ₂ O _m	E ₄₅₀₀ OH	E ₃₄₅₀ H ₂ O _t	E ₂₃₅₀ CO _{2 m}	E ₁₆₃₀ H ₂ O _m	Source
Rhyolite	1.61	1.73	56–100 ^a	1214	55	Newman et al. [1986] Behrens et al. [2004]
Dacite	1.2	1.05	68	1066	55	Ohlhorst et al. [2001] Yamashita et al. [1997] Wysoczanski and Tani [2006] Moore et al. [2000]
Andesite	1.08	1.15	62	945	43	King et al. [2002] Mandeville et al. [2002]
Basaltic andesite	0.75	0.65	61	n/a	42	Ohlhorst et al. [2001] Mandeville et al. [2002]

^aThe E₃₄₅₀ extinction coefficient is a function of the partitioning between H₂O_m and OH. Other spectra from the same sample set, where the A₅₂₀₀ and A₄₅₀₀ peaks were visible, were used to determine the partitioning.

and 2350 cm⁻¹ (CO_{2 m}) peaks were obtained using a flat baseline [King et al., 2002]. The size, thickness, and composition of the melt inclusion determined which peaks were visible and viable. Normally, the absorbance of the 3450 cm⁻¹ peak was less than 1. However, in rare instances, this absorbance was between 1 and 1.5. If the top of the peak was not flattened due to saturation and the noise level was low, it was deemed usable following Newman et al. [1986]. To enable low detection limits for CO₂, the entire instrument was placed in a protective shroud and purged using high-purity nitrogen gas. The atmospheric CO₂ concentration within the shroud was measured at less than 50 ppm using a Green Eye CO₂ room analyzer. Using silicic and basaltic glass standards, we determined the practical detection limits for H₂O at 50 ppm and 10 ppm for CO₂. For melt inclusions of basaltic andesite compositions, the 1400–1500 cm⁻¹ range was examined for carbonate peaks (CO₃²⁻). Due to the curved background and the interference from the 1630 cm⁻¹ peak, our limit of detection for carbonate is estimated at ~20 ppm. Concentrations of CO₂ and H₂O were calculated using Beer's Law from Newman et al. [1986]:

$$wt\% = MA / (\epsilon d \rho)$$

where *M* is the molar mass of CO₂ or H₂O (g mol⁻¹), *A* is the absorption for the peak of interest, ϵ is the extinction coefficient for the peak (mol⁻¹ cm⁻¹), *d* is the thickness of the wafer (cm), and ρ is the density of the glass in question (g L⁻¹). The density calculation incorporated water data and was performed iteratively following a model by Lange [1997]. The list of extinction coefficients, their associated errors and corresponding peaks are shown in Table 1. Sample thickness was measured using the FTIR stage calibrated against a digital micrometer. The interference fringe method showed good agreement with the stage method.

Errors in the calculation of H₂O and CO₂ concentrations are associated primarily with the measurement of absorption (± 2 –20%) and wafer thickness (± 5 μ m or ~5–15%). The error in thickness measurements is similar for all our samples, but absorption errors increase with small melt inclusions. Using replicate measurements of glass standards (M6N, M3N, and PCD from Devine et al. [1995]; EXP51 from Mangan and Sisson [2000]) at an aperture of 100 μ m, we can reproduce absorption on the order of ± 0.0001 (2 σ). This places our best error estimate at ± 0.05 wt % for H₂O and ± 5 ppm for CO₂. To obtain reliable measurements of melt inclusion glass, without any interference from the host crystal, we reduced the aperture diameter, which increases the noise of the spectra. By measuring the same melt inclusion 3 times, we eliminated the need for smoothing, but the increased noise level is reflected in the increased error of the absorption (up to ± 20 %). In this worst-case scenario, we estimate our error at ± 0.9 wt % for H₂O and ± 15 ppm for CO₂. However, the large majority of samples have absorption errors which are much smaller, on the order of ± 2 –5%. In this case, we estimate our error at ± 0.05 wt % for H₂O and ± 2 ppm for CO₂. There is also an inherent error in our selection of extinction coefficients, especially when dealing with a large range in composition such as for Hekla. These were selected to represent the most accepted values (Table 1).

3.3. Electron Microprobe Analysis

Major elements in matrix glasses, olivines, and melt inclusions, as well as S and Cl in matrix glasses and melt inclusions, were acquired using a JEOL 8900 electron microprobe at McGill University. To minimize Na loss for glasses, we used an accelerating voltage of 15 kV, a current of 2 nA, and a defocused beam diameter of 15 μ A. Counting times for Na were 15 s, 60 s for Cl, 120 s for S, and 20 s for Si, Ti, Al, Fe, Mn, Mg, K, and P. In

order to improve detection limits for volatiles, we measured up to three points within a single melt inclusion using the accumulation method. Analyses were performed by counting the peak first, followed by background to the left and right. In order to prevent Na loss during analysis, the condition file was set up and tested by looking at the Na count versus time.

The practical detection limits for S and Cl were determined using repeat measurements on glass standards. Using KN9 [Stix *et al.*, 1995] as the Cl standard and NBS620 as the S standard, we were able to define our lowest reproducible concentrations as ~ 90 ppm for S and ~ 80 ppm for Cl. Repeat analyses of mineral and glass standards within a single analytical run produced an accuracy of 5% for major elements at concentrations > 1 wt %. We used M6N, M3N, PCD, and 35-1 [Devine *et al.*, 1995] as secondary standards for major elements. Since these standards are principally characterized for different levels of H₂O, we also used them for the volatiles-by-difference method [Devine *et al.*, 1995; Humphreys *et al.*, 2006; Longpré *et al.*, 2014] to compare H₂O results between the FTIR and electron microprobe (supporting information Figure S1). Accepted values for major element, S, and Cl standards are presented in supporting information Table S1.

Olivine crystals were analyzed for major elements using an accelerating voltage of 20 kV, a current of 30 nA and a beam size of 5 μm . Counting times for Ca were 60 s, 40 s for Ni and 20 s for Si, Ti, Al, Fe, Mn, Mg, and Cr. The olivine standard used was supplied by CM Taylor Company Supplies. For each olivine grain, three points were collected: one in the core, one close to the rim, and one located between the first two and near an analyzed melt inclusion.

4. Results

4.1. Petrography and Mineralogy

Tephra from all four eruptions are characterized by a mineral assemblage of plagioclase, olivine, clinopyroxene, ilmenite, magnetite, and zircon (in order of modal percentage). In more evolved tephra (1104 and H3), we also observed apatite and pyrrhotite. In contrast to stratigraphic variations in crystal content observed at many other fall deposits [e.g., Hildreth and Wilson, 2007], the first erupted material for zoned eruptions is comparatively crystal rich ($\sim 10\%$), while the last erupted material tends to be crystal poor ($\sim < 1\%$). Products from evolved eruptions (H3 and 1104) tend to be more crystal rich (1–10%) than their more primitive counterparts (1–3%) (1845 and 1991). Sulfides were observed as inclusions in olivine crystals from H3 and 1104. They are present in trace amounts in both eruptions with no clear difference in abundance between the first and last erupted material.

Olivine compositions correlate strongly with the composition of the deposit and range from Fo_{11–13} in rhyolites, Fo_{22–26} in dacites, Fo_{41–44} in andesites to Fo_{58–60} in basaltic andesites (Figure 4). This excellent correlation indicates that the crystals are phenocrysts rather than antecrysts or xenocrysts. Within a single eruption, the variability is largest in H3 where the rhyolitic base has olivines of Fo₁₃, while the dacitic light and dark top have forsterite contents that range from Fo₂₂ to Fo₂₆. Minor Fo zonation is present in the olivines of H3 light and dark top (1–2 mol %), but generally there is no obvious zonation in any of the other olivines. One olivine of Fo₁₃ was found in H3 dark top, a unit where olivines of \sim Fo₂₅ are dominant. Olivine grains commonly contain inclusions of ilmenite, magnetite, zircon, and needle-like growths of apatite. Such inclusions are more common within olivines of the more evolved deposits.

Melt inclusions in evolved deposits (H3 and 1104) were observed in plagioclase, olivine, and clinopyroxene and restricted to plagioclase and olivine in less evolved eruptions (no clinopyroxene was present in the 1845 and 1991 deposits). Olivine grains selected for analysis came from the 1400–710 and 710–500 μm size fractions, with no evidence of multiple populations. Two types of melt inclusions were observed within the olivines. The first type consists of clear, spherical, 20–150 μm inclusions with or without a vapor bubble (1–5 μm). These inclusions are restricted to rhyolites. The second type of melt inclusion is darker in color, also 20–150 μm in size, and occurs as irregular fluid-like shapes commonly containing a vapor bubble (1–10 μm). This second type of darker melt inclusions first appears in olivines from dacite deposits (H3 light top) and becomes the dominant melt inclusion type in H3 dark top, 1845 and 1991. H3 light top is the only deposit where both types of melt inclusions are found. They are never found within the same olivine grain, but may be found in different olivines from the same pumice lump. Despite their visual differences, the two types are indistinguishable in major element and volatile concentrations (see below). Melt inclusions with

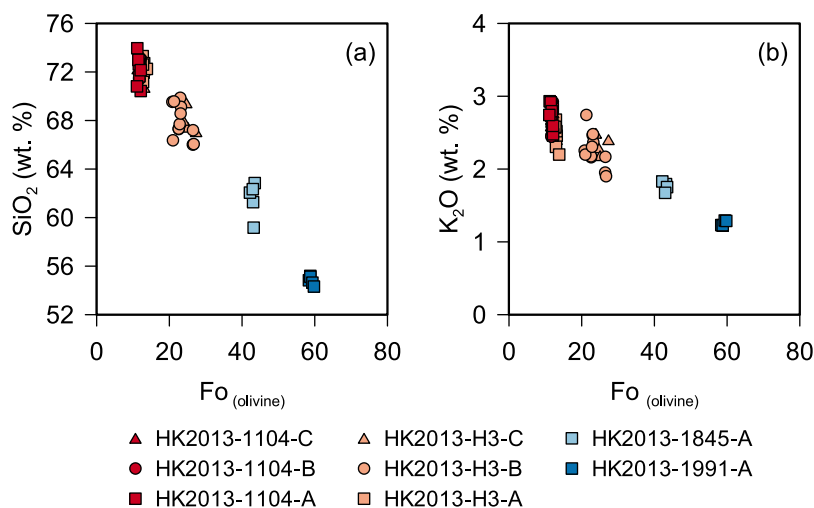


Figure 4. Forsterite contents of olivines plotted versus (a) SiO₂ and (b) K₂O contents of their olivine-hosted melt inclusions. Four distinct populations of melt inclusions are present in basaltic andesite (Fo ~60), andesite (Fo ~42), dacite (Fo ~20-25), and rhyolite (Fo 11). The color coding and symbols reflect samples from different eruptions (red, orange, light blue, and dark blue) and sampling horizons within the same eruption (square = base, circle = light top, and triangle = dark top). These symbols and color codes are the same for all other figures.

vapor bubbles were excluded during sample preparation and were not analyzed, in order to avoid any potential loss of volatiles such as CO₂.

4.2. Major Elements

Melt inclusions and matrix glasses were normalized volatile free for the purposes of comparison (Figure 5). Matrix glass compositions range from rhyolite (72.7 wt % SiO₂) to basaltic andesite (54.6 wt % SiO₂). Deposits from the largest-volume zoned eruption, H3, contains rhyolite glass at the base (72.2 wt % SiO₂) and dacite glass at the top (64.5 wt % SiO₂). The change from white pumice at the base to pink pumice at the top of the deposit is associated with a change in iron content from 3.40 wt % to 7.38 ± 0.10 wt % FeO*. The 1104 deposit, which is visually zoned in the field, lacks a corresponding chemical zonation. Instead, matrix glass is rhyolitic throughout, and the visual zoning results from an upward decrease in pumice vesicularity. The H3 deposit has a similar upward decrease in vesicularity. Matrix glasses of 1845 and 1991 tephra are andesitic (61.4 ± 0.7 wt % SiO₂) and basaltic andesitic (54.8 ± 0.4 wt % SiO₂), respectively.

Olivine-hosted melt inclusions range similarly in SiO₂ concentration (73.9–54.3 wt %). The zoned nature of H3 recorded in its matrix glasses is also recorded in its melt inclusions (73.3–64.4 wt % SiO₂). Melt inclusions from the 1104 deposit are dominated by rhyolite and show the same lack of zonation as do the matrix glasses (73.9–70.4 wt % SiO₂). Matrix glass and melt inclusion compositions are also similar for the 1845 and 1991 eruptions. In general, major element compositions in melt inclusions define trends consistent with

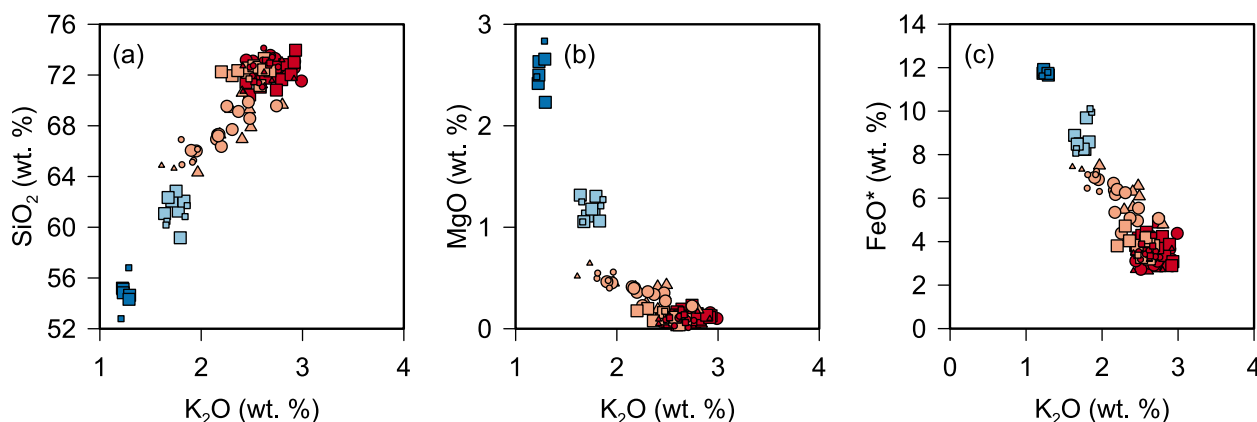


Figure 5. Select major oxide concentrations for melt inclusions (large symbols) and matrix glasses (small symbols).

magmatic evolution through fractional crystallization. Inflections in P_2O_5 , Al_2O_3 , and CaO (and MgO) mark the onset of apatite, feldspar, and clinopyroxene crystallization, respectively.

A notable feature of Hekla's most evolved products is the diversity in K_2O concentration of glasses (Figure 5). This is most evident in melt inclusions with high SiO_2 and low MgO concentrations. In H3, K_2O ranges from 2.4 to 2.9 wt % in H3 base and 1.9–2.7 wt % in H3 dark top. For 1104, the range in K_2O is 2.4–2.9 wt %. The larger range in K_2O for H3 is due to the wider range of magma compositions. Similar trends in K_2O and other major oxides are observed in matrix glasses as well, but the magnitude of this variability is smaller (Figure 5). One notable difference between matrix glasses and melt inclusions, most prominent for SiO_2 and K_2O , stands out. Melt inclusion compositions from H3 form a near-continuous array spanning between 1845 and 1104 glasses. Matrix glass compositions on the other hand form a gap between 66.9–70.8 wt % SiO_2 and 1.97–2.41 wt % K_2O .

Olivine-melt inclusion and olivine-matrix glass equilibria were examined using the following equation from Roeder and Emslie [1970] and Toplis [2005]:

$$Kd_{OL-Melt} = \frac{X_{OL}^{Fe} / X_{OL}^{Mg}}{X_{Melt}^{Fe} / X_{Melt}^{Mg}}$$

where $X_{OL}^{Fe} / X_{OL}^{Mg}$ is the ratio of Fe to Mg in olivine and $X_{Melt}^{Fe} / X_{Melt}^{Mg}$ is the ratio of Fe to Mg in the melt. The Kd ratio is typically used for melts of mafic compositions [Toplis, 2005], but studies at Hekla [Portnyagin *et al.*, 2012] and other volcanoes (e.g., Parícutin volcano in Mexico [Erlund *et al.*, 2010]) [Rowe *et al.*, 2011] have applied it for more silicic compositions as well. Given the dependence of this ratio on complex parameters such as temperature and water content of the liquid, Toplis [2005] proposed a possible expansion of the equilibrium range of Kd values from 0.3–0.4 to 0.15–0.45 for more evolved compositions (up to 60 wt % SiO_2). Clearly, caution is warranted here on how this parameter is applied to magmas of evolved compositions. For our study, if the Kd value of a sample fell outside the expanded 0.15–0.45 range, it was removed from further consideration (supporting information Figure S2).

A majority of the melt inclusions (45 olivines of a total of 65) have Kd values of 0.3–0.4, suggesting they are in equilibrium with their host olivines and have experienced no postentrapment crystallization [Toplis and Carroll, 1995]. Variability in the Kd ratio increases for olivines in more silicic melt inclusions and may be attributed to lower MgO concentrations (0.1–0.5 wt %). These values approach the detection limit of the electron microprobe and decrease the accuracy from better than 5% (>1 wt %) to better than 10% (<1 wt %). The Kd range is lowest in 1845 (0.29–0.33) and greatest in 1104 (0.14–0.5), the most silicic end-member. Kd values of olivines versus matrix glasses show more variability. H3 dark top is dominated by olivines of Fo_{25} which have Kd values of ~ 0.45 . One anomalous olivine from this sample has a composition of Fo_{13} and a resulting Kd of 0.9. This anomalous olivine likely was part of the magma of H3 base and may be considered a xenocryst, thus excluding it from H3 dark top. All other olivine-matrix glass Kd values are in the 0.3–0.4 range, suggesting they are in equilibrium.

Postentrapment crystallization of olivine along the rims of melt inclusions along with diffusion of H could lead to variability in the major element composition and volatile contents of melt inclusions [Gaetani *et al.*, 2012; Portnyagin *et al.*, 2008; Hartley *et al.*, 2016]. Inspection of melt inclusion rims under optical microscope and electron back-scatter imaging does not reveal the presence of any newly crystallizing rim. Furthermore, if new rims had crystallized, we would expect to see variability in the Fe-Mg content of the melt inclusions as well as an increase in incompatible elements such as K_2O and H_2O . Slight variability in the Kd ratio within the acceptable range (0.15–0.45) could be a result of minor postentrapment crystallization, leading to variable K_2O . However, variable H_2O/K_2O ratios within a single eruption or even part of an eruption sequence (e.g., 1104 dark top) suggest the presence of an additional process.

4.3. Volatile Components

Melt inclusions from the four deposits record a wide range of volatile contents. Water concentrations are highest in the first erupted material of the most evolved eruptions, tending to be lower for the last erupted magma. The evolved deposits are more variable in terms of major elements, H_2O , S, and Cl. Last, melt inclusions record very little to undetectable CO_2 for all four deposits.

4.3.1. H₂O and CO₂

The full suite of melt inclusions from the four deposits ranges in concentration from 0.8 to 5.67 wt % H₂O (Figure 6). The most water-rich melt inclusions are from the H3 and 1104 deposits, and these deposits also preserve the largest range in preeruptive water contents. The melt inclusions from the 1845 and 1991 deposits represent less evolved melts, contain less water on average than their silicic counterparts, and the absolute range in concentrations is also smaller. However, the relative range of water concentrations about the mean values of 1845 and 1991 reveal a similar range to 1104 and H3 (see below). The deposits of 1845 and 1991 contain fewer olivines, so the smaller range may partly reflect fewer analyzed samples. Overall, the increase of water correlates positively with SiO₂ and K₂O and negatively with the forsterite content of the host olivine (Figures 6 and 8).

Within the H3 and 1104 melt inclusions, we observe a large diversity in dissolved water throughout the individual deposits and a general decrease from the base to the top of the deposit. In H3, the average water concentrations for the base, light top and dark top are 4.57, 2.38, and 2.27 wt %, respectively. The range of water concentrations also decreases from 3.36 to 5.57 wt % at the base to 1.35–3.05 wt % for the light top and 1.63–2.97 wt % at the dark top. If we consider the relative ranges for H3 base (48%), light top (62%) and

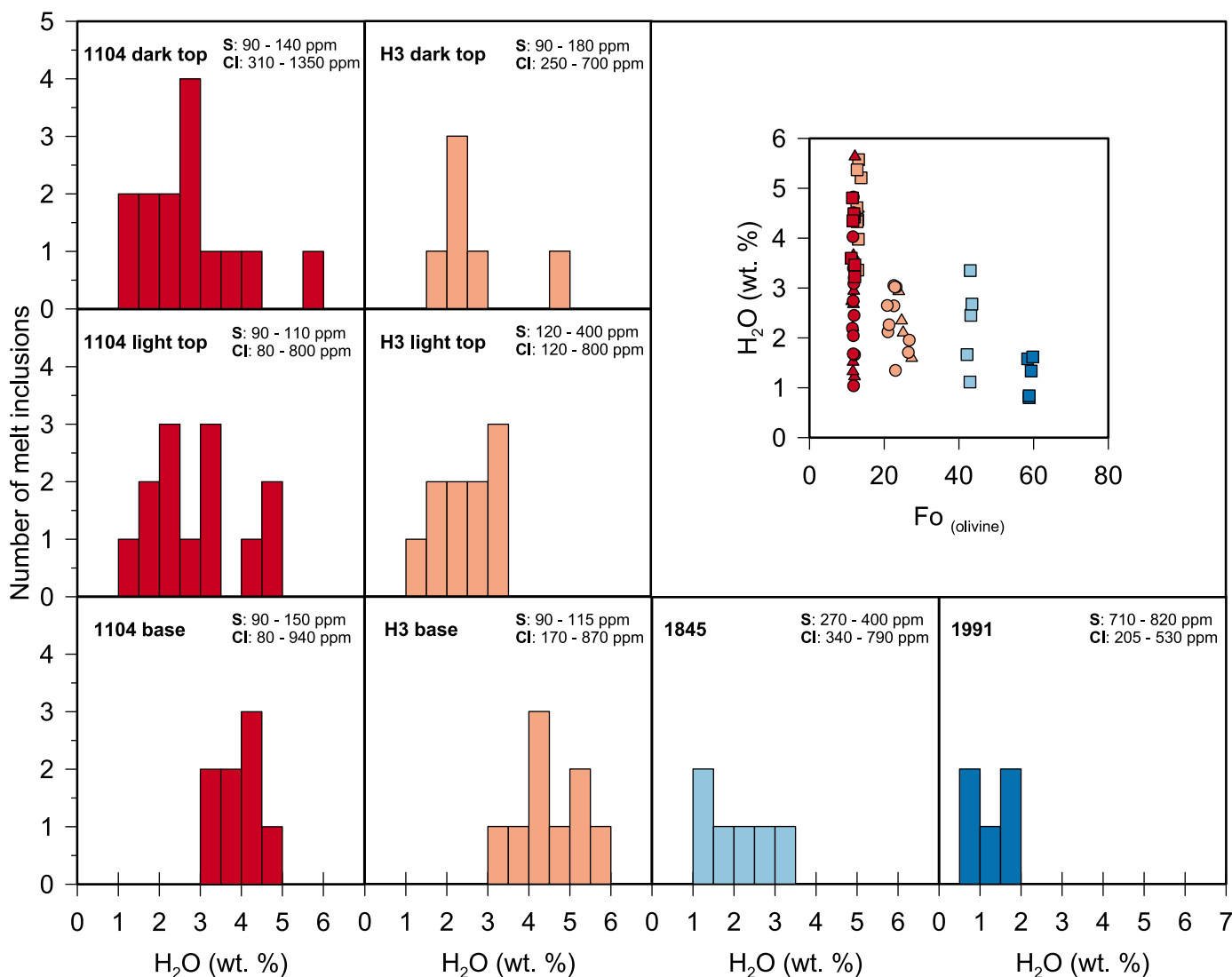


Figure 6. Histograms of H₂O concentrations and Fo contents of olivines plotted versus H₂O concentrations in melt inclusions. The first erupted material at the base of the stratigraphic section is located at the bottom of the figure. The range in S and Cl concentrations of each horizon are included for reference. Note the decrease in average H₂O concentrations from the first erupted to the last erupted material for the silicic eruptions.

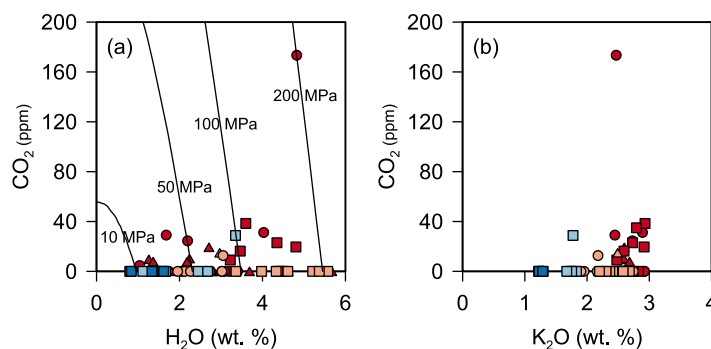


Figure 7. H₂O versus CO₂ concentrations in melt inclusions. (a) The 200, 100, 50, and 10 MPa isobars were calculated for a rhyolitic melts of a similar composition to 1104 at 950°C using VolatileCalc [Newman and Lowenstern, 2002]. This composition and temperature [Putirka, 2008] were selected to represent the conditions at which melt inclusions were being trapped within 1104, the most CO₂-rich deposit. The sample with the highest water content (5.67 wt %) and the sample with the highest CO₂ content (4.82 wt % H₂O and 173 ppm CO₂) both give vapor saturation pressures of ~200 MPa. (b) Plot of K₂O versus CO₂ demonstrating the increased occurrence of CO₂ in more evolved magmas.

dark top (62%), the wetter melts are no more diverse than the drier ones. There is a single melt inclusion in H3 dark top with a water content of 4.62 wt %, which is hosted in an olivine with a composition of Fo₁₃. Both these values clearly indicate that this crystal originated from the H3 base.

For 1104, the average water concentration for the base, light top, and dark top is 4.01, 2.84, and 2.77 wt %, respectively. In contrast to H3, the range in water concentrations in 1104 increases with stratigraphic height from 3.22 to 4.01 wt % at the base to 1.04–4.82 wt % for the light top

and 1.26–5.67 wt % for the dark top. The same increase is reflected in the standard deviation relative to the means with 14%, 41%, and 44%, respectively.

Samples from 1845 and 1991 were collected only from their base, hence represent the first erupted material. Their average water concentrations are 2.11 wt % in 1845 and 1.23 wt % in 1991. Their concentrations range from 1.12 to 3.35 wt % in 1845 and 0.80 to 1.62 wt % in 1991.

Our FTIR analyses for the four eruptions of various compositions demonstrate that there is very little to no detectable CO₂ preserved in the melt inclusions (Figure 7). The small amounts which were detected mark the first direct measurements of CO₂ at Hekla. Given how rare CO₂ is, we assessed its content within eruptions based on how often it was detected and in what quantities. CO₂ was measured in 7 out of 10 samples in 1104 base ranging from 9 to 38 ppm, in 5 of 13 samples in 1104 light top (5–173 ppm) and in 5 of 14 samples in 1104 dark top (8–19 ppm). No carbonate (CO₃²⁻) was detected in any sample. The only other instances where molecular CO₂ was detected was one melt inclusion in H3 light top (13 ppm), one melt inclusion in H3 dark top (15 ppm), and one melt inclusion in 1845 (29 ppm).

4.3.2. S and Cl

Sulfur concentrations in melt inclusions range from below detection limit to 820 ppm (Figures 6 and 8). Melt inclusion sulfur concentrations decrease with increasing SiO₂, K₂O, and H₂O, and increase with

FeO (Figure 9). The 1991 melt inclusions are the most sulfur rich (715–820 ppm), followed by 1845 (270–400 ppm), and H3 light and dark top (maximum of 400 ppm). The other H3 and 1104 melt inclusions cluster at low sulfur concentrations (maximum 150 ppm), many of which are below the ~90 ppm detection limit for S. Except for the zoned H3 deposit, where S varies from an average of <90 ppm at the base to 205 ppm in light top and <90 ppm in dark top, we observe no clear variability stratigraphically for S in melt inclusions.

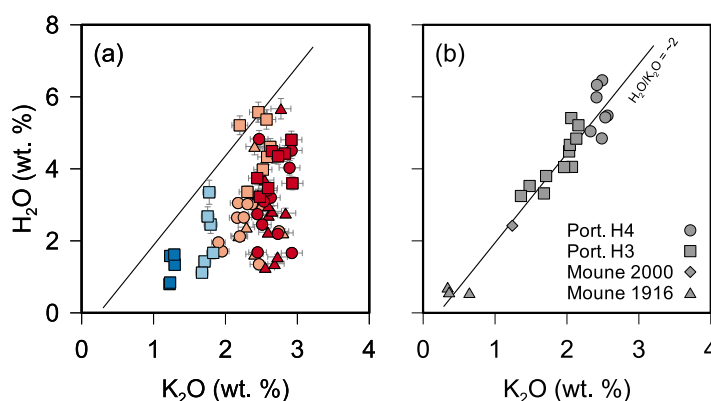


Figure 8. The H₂O/K₂O ratio of melt inclusions from (a) this study and (b) from the 1916 and 2000 deposits [Moune et al., 2007] and H3 and H4 deposits [Portnyagin et al., 2012]. The straight line is defined by the reported H₂O/K₂O ratio of ~2 from previous studies (Figure 8b) and is included on the left (Figure 8a) for reference. Note the variability in the H₂O/K₂O ratio as well as lower ratios for later erupted 1104 and H3 melt inclusions, suggesting loss of water through degassing.

Chlorine concentrations in melt inclusions are diverse in all four

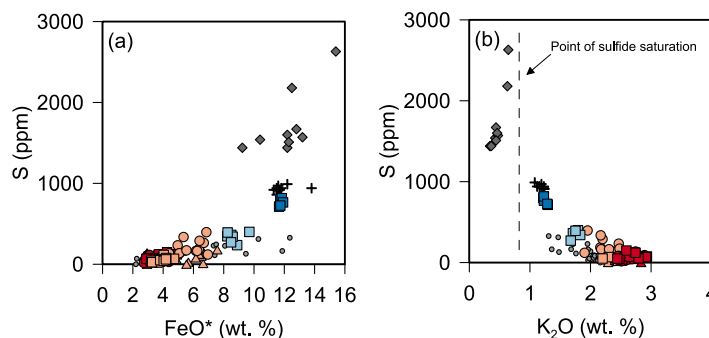


Figure 9. (a) Positive correlation between FeO^* and S for melt inclusions from this study (colored symbols), select samples from the 1916 basaltic eruption (grey diamonds), and the 2000 basaltic andesite (grey crosses) from *Moune et al.* [2007], and the H3 and H4 eruptions (grey circles) from *Portnyagin et al.* [2012]. (b) Early in the evolution of Hekla magmas, S behaves incompatibly and increases with K_2O . Once sulfide saturation occurs at ~ 0.7 to 0.8 wt % K_2O , the S content decreases steadily with increasing K_2O [*Moune et al.*, 2007]. Many samples from the silicic eruptions are at or below the detection limits for S (~ 90 ppm).

eruptions (Figures 6 and 8). The 1991 and 1845 melt inclusions have more restricted Cl ranges (205–530 and 335–790 ppm, respectively), whereas H3 and 1104 show a wider range (150–1350 ppm). The 1104 melt inclusions have consistent ranges in Cl (~ 900 ppm) and greater Cl contents (1350 ppm) than for H3, where the highest concentration is 870 ppm and the range in chlorine varies from 700 ppm in H3 base to 450 ppm in H3 dark top.

Within the prepared olivine grains, there are 12 instances in which a single grain holds more

than one melt inclusion: one instance from 1104 base, five from 1104 light top, four from 1104 dark top, and one each from H3 light top and dark top. It is difficult to assess whether the occurrence of multiple melt inclusions in 1104 is an unusual feature of this eruption or simply a reflection of the quality and size of melt inclusions. We observed multiple melt inclusions in a single grain of olivine in other deposits as well, but they were either too difficult to expose simultaneously or too small for FTIR analysis. In 5 of the 12 cases, water concentrations differ by less than 0.8 wt %. In six cases, the difference is ~ 0.8 wt %. In only one case, the difference is on the order of 4.4 wt %. In all 12 instances, the change from higher to lower water concentrations is also reflected in an increase in sulfur. This negative correlation between water and sulfur is not accompanied by obvious differences in major oxides such as SiO_2 , K_2O , FeO, etc.

5. Discussion

5.1. H_2O in Hekla Magmas

Maximum water contents in melt inclusions increase from 1.62 wt % for the 1991 deposit, through 3.35 wt % for 1845, to 5.57 wt % in H3 and 5.67 wt % in 1104. In this respect, the maximum water content in Hekla melts appears to be a function of magmatic evolution. *Portnyagin et al.* [2012] demonstrated that the entire range of Hekla water concentrations (~ 0.2 to ~ 6 wt % H_2O) can be accounted for by 90% of crystallization of parental mafic magmas containing 0.6 wt % H_2O . In addition to water, potassium also behaves as an incompatible element in Hekla magmas; its increase in more evolved magmas is also suggestive of fractional crystallization. From previous studies, the $\text{H}_2\text{O}/\text{K}_2\text{O}$ ratio for Hekla magmas, both basaltic and rhyolitic, has been established at 2–2.3 [*Moune et al.*, 2007; *Portnyagin et al.*, 2012]. However, according to our data set, only the first erupted material of the more evolved eruption approaches this value (Figure 8). Melt inclusions from 1991, 1845, and later erupted 1104 and H3 all display lower $\text{H}_2\text{O}/\text{K}_2\text{O}$.

The large, silicic deposits (e.g., H3 and 1104) show a decrease in the water contents between the first erupted and the last erupted melt inclusions. The average decrease between base and light top in both H3 and 1104 is on the order of 2.2 wt %. This decrease in water content is not restricted to melt inclusions in different olivine grains; it also can be observed in multiple melt inclusions within a single olivine grain. In the 1104 deposit, a single grain from the base with two melt inclusions records water contents of 4.81 and 4.35 wt %, while a grain from 1104 dark top records water contents of 5.67 and 1.26 wt %. As a result, the full range of water contents in H3 and 1104 is on the order of ~ 4 wt %. This is a notable feature of Hekla's more evolved melts and may result from (1) trapping melts at various stages of evolution, (2) diffusion of H through the olivine lattice, (3) syneruptive degassing, (4) melt entrapment at different pressures, or (5) a combination of these processes.

If fractional crystallization controls the amount of water within the melt, then lower water contents should be associated with less evolved melts. However, within a single deposit sequence of similar composition

(e.g., 1104), we observe a wide range in water contents, with variable H₂O/K₂O ratios and no significant variability in other major elements, such as K₂O. It is therefore unlikely that melts are being trapped at various stages of fractionation within a single eruption. Careful examination of melt inclusions under the microscope did not reveal the presence of cracks or any other evidence of leakage, and any grain in which leakage was suspected was discarded. *Gaetani et al.* [2012] reported that diffusion of H from melt inclusions in olivines may occur on the order of hours or days. Given the long residence times and differentiation time scales on the order of hundreds to thousands of years for closed-system fractionation at Hekla [*Chekol et al.*, 2011], diffusion of H before or during eruption could lead to a decrease in water contents. However, if H diffusion were occurring over these extended time intervals, then prior to eruption all melt inclusions located at the same level within the magma chamber should have similar water contents. Our ~4 wt % range of water content within a single eruption argues against this type of diffusion. If melt inclusions reflect syneruptive degassing, then olivines crystallized during magma ascent and trapped pockets of melt that were variably degassed. Unlike fractional crystallization, the change in the composition of the melt and the Fo content of olivines would be minimal in this case. This is consistent with our data set. Syneruptive depressurization may produce a wide range in water contents [*Myers et al.*, 2014; *Soule et al.*, 2012]; such a process should be strongly coupled to syneruptive degassing. Last, the range in water content may reflect movement of magma within the crust and trapping of melts at different pressures or depths.

5.2. Are Magmas at Hekla Volatile Saturated?

During fractional crystallization of volatile-undersaturated magma, water behaves as an incompatible component, increasing its concentration in more evolved melts. The first erupted material from H3 and 1104, with the highest H₂O contents, may represent a magma which is closest to volatile saturation at Hekla. Repose intervals for eruptions in our data set range from 10 years for 1991, 79 years for 1845, ~250 years for 1104, and 100–500 years for H3. The repose periods for H3 and 1104 are potentially different, as are their volumes, yet the H₂O contents of the first erupted material are similar, suggesting that the ~5.5 wt % water could be close to a saturation threshold for more evolved compositions. However, water contents of ~6.2 wt % have been reported for the H4 eruption [*Portnyagin et al.*, 2012], with a repose interval of ~500 years. This increasing trend in water contents, even for the most evolved eruptions, brings into question the ultimate saturation limit of Hekla magmas.

Using the CO₂/Nb ratio (314 ± 125), *Hauri et al.* [2002] estimated the CO₂ concentration of the depleted mantle beneath Iceland at 140 ± 56 ppm. *Hartley et al.* [2014] reported a large variation in the CO₂/Nb ratio (3.8–364) within melt inclusions from the neighboring 1783–1784 Laki fissure eruption. They concluded that the magmatic system was supplied by a combination of enriched and depleted primary melts. *Neave et al.* [2015] reported a CO₂/Nb ratio of 159 ± 74 from plagioclase-hosted melt inclusions from the 10 ka Grímsvötn tephra and concluded that the lower ratio reflects CO₂ saturation prior to eruption. *Portnyagin et al.* [2012] reported Nb concentrations of 60–80 ppm in melt inclusions from the H3 deposit and 70–90 ppm in H4. Using these values and our measurements of CO₂ in H3 (<10–15 ppm) and 1104 (<10–173), we estimate the CO₂/Nb as 0.7–0.75 and 0.2–8, respectively. If fractional crystallization is responsible for the formation of Hekla's more evolved magmas (1104, H3 and H4), then using a CO₂/Nb ratio of ~300 predicts a CO₂ content of 1.5–4 wt CO₂ in the most evolved magmas. The stark contrast between predicted and observed CO₂/Nb ratios and the absence of CO₂ and carbonate (CO₃²⁻) are suggestive of two scenarios: (1) most of the CO₂ was lost through degassing during magma ascent and/or isobaric degassing, (2) CO₂ was lost during solidification and remelting of previous intrusions deeper within the crust, or (3) both hold true.

Melt inclusions from the 1916 eruption are a good representation of the least evolved end-member erupted from Hekla. Its basaltic composition suggests that this magma underwent low degrees of fractional crystallization in the crust and is likely the closest representation of the basaltic source. *Moune et al.* [2007] compared the volatile evolution between the 1916 basalt and the 2000 basaltic andesite, concluding that H₂O and F were not removed from the melt prior to entrapment, but Cl and S were. Sulfur concentrations of 2200–2600 ppm in the 1916 melt inclusions demonstrate that sulfur initially behaves as an incompatible element, increasing in concentration along with H₂O and K₂O in the melt. Once the melt has evolved to the point that iron oxides, such as titanomagnetite begin to crystallize, the FeO content of the melt begins to decrease [*Baker and Moretti*, 2011]. As a result, the system reaches sulfide saturation, and the sulfur content of the melt declines from a high of ~2700 ppm in 1916 (~47.0 wt % SiO₂) to a high of ~900 ppm in 2000 (54.2 wt % SiO₂). Our S data set extends the trend established by *Moune et al.* [2007] from basaltic andesite

compositions (e.g., 1991) to rhyolites (e.g., H3 and 1104). We observe a continuous S decrease as K₂O increases in the melt inclusions (Figures 8 and 9a). This trend correlates with decreasing FeO in the melt due to continued olivine and iron oxide crystallization. Significantly, we observe the presence of pyrrhotite in more evolved magmas (1104 and H3).

Using the SolEx model [Witham *et al.*, 2012] for basaltic compositions at a temperature of 1050°C obtained using the olivine-melt thermometer [Putirka, 2008], and oxygen fugacity at FMQ [Baldrige *et al.*, 1973; Moune *et al.*, 2007], we observe the onset of H₂O and S degassing at ~15–20 MPa. These low pressures demonstrate that the decrease in S within the melt is most likely due to sulfide saturation and not degassing.

Reports of recent historic eruptions and analysis of past deposits have noted the explosive nature of the initial phase of eruptions at Hekla. It is likely that both passive degassing at depth associated with cooling bodies [Wallace *et al.*, 1995] as well as degassing during ascent [Moune *et al.*, 2007] contribute to the development of a preeruptive vapor phase. The formation of such an exsolved gas phase would suggest that melts at Hekla do achieve volatile saturation. Furthermore, despite the trend of increasing water contents in more evolved melts, the almost complete lack of CO₂ further supports the model of volatile saturation within the crust. To explore the range in volatiles and to determine when saturation might occur, we examine models of magma generation at Hekla.

5.3. Magma Evolution at Hekla

Thorarinsson [1967] discovered that the degree of magmatic evolution at Hekla is related to the repose interval between eruptions. Major element variations from this study and others [Sigmarsson *et al.*, 1992; Sverrisdottir, 2007; Moune *et al.*, 2007; Chekol *et al.*, 2011; Portnyagin *et al.*, 2012] indicate that this evolution is one principally of fractional crystallization, the extent of which is dependent on time. Hence, concentrations of incompatible components, such as K₂O, increase systematically from less evolved magmas to more evolved magmas (Figure 5). The range in incompatible components, such as K₂O and H₂O within zoned and unzoned deposits, and the lack of CO₂ suggests the presence of a secondary process of evolution, such as assimilation, magma mixing, or possibly a combination of the two [Nicholson *et al.*, 1991; Cioni *et al.*, 1995; de Silva and Wolff, 1995; Costa and Singer, 2002]. Basaltic magmas stored in reservoirs in the lower crust and near the crust-mantle boundary (~24 km) have been proposed [Chekol *et al.*, 2011] and modeled using GPS deformation [Geirsson *et al.*, 2012]. It is possible that these magmas cool and solidify in the lower crust, losing their CO₂ in the process. Subsequent intrusions melt these gabbroic intrusives and release water bound in amphiboles, further facilitating partial melting. Such a scenario would explain the lack of CO₂ in magmas erupted at Hekla, both mafic and felsic.

Crustal rocks in the southern part of Iceland are primarily metabasalts (gabbros) of the zeolite facies that transition to greenschist facies at depth [Walker, 1960], and/or preexisting silicic intrusive rocks [Sigmarsson *et al.*, 1992]. The ⁸⁷Sr/⁸⁶Sr and ²³⁰Th/²³²Th systematics of Hekla lavas suggests that only recent dacites (e.g., 2000 pumice fall) have assimilated silicic intrusives and that older dacites and rhyolites (e.g., H3 and 1104) evolved principally through fractional crystallization and crustal assimilation of older metabasalts [Chekol *et al.*, 2011]. Hydrothermal alteration of metabasalt host rocks (low-K greenstone) may alter the alkali content due to their high mobility during leaching and ion exchange [Wood *et al.*, 1976; Von Damm, 1990; Hildreth and Wilson, 2007; Zellmer *et al.*, 2008]. Hydrothermally altered crustal rocks of the Icelandic rift zone are typically characterized by low δ¹⁸O [Hattori and Muehlenbachs, 1982; Sveinbjörnsdottir *et al.*, 1986]. If magmas are assimilating such rocks, the resulting compositions will be depleted in δ¹⁸O. The same holds for partial melting. Hekla magmas exhibit a δ¹⁸O range from 4.5 to 5.3‰ [Sigmarsson *et al.*, 1992]; when restricted to dacites and rhyolites, the range remains nearly identical (4.9–5.2‰). These values are close to those of the mantle, suggesting that either Hekla magmas have assimilated little to no crustal material or the host rock or source is not very depleted in δ¹⁸O. U-Th disequilibria ages from zircons from the 1158 eruption reveal that many predate the age of the eruption by 10³–10⁵ years. The δ¹⁸O composition of these zircons varies between ~1.2 and 5‰, suggesting that host rocks at Hekla vary in both age and level of δ¹⁸O depletion [Bindeman *et al.*, 2012]. The most likely cause of this depletion is high-temperature alteration of crustal rocks at high temperature which produces rocks with δ¹⁸O in the ~2–5‰ range. It is therefore possible that more hydrothermally altered crust was assimilated in Hekla's early history when the

plumbing network was being established, but this no longer seems to be the dominant form of magmatic and volatile evolution.

Models of silicic magma generation at Hekla by *Sigmarsson et al.* [1992], *Sverrisdottir* [2007], and *Chekol et al.* [2011] explore the role of assimilation of previous silicic intrusives. Given the size and frequency of large silicic eruptions in Holocene times, it seems plausible that Hekla's plumbing network undergoes interaction between fresh injections of basaltic andesite and cooling dacitic/rhyolitic bodies (e.g., Okmok Volcano, Alaska) [Finney et al., 2008]. These bodies might form from magmas that have stalled in the crust or residue from smaller silicic eruptions such as 1104, whose lack of zoned deposit suggests that only part of the magma chamber was emptied. Furthermore, the model of magma generation suggested by *Portnyagin et al.* [2012] requires 90% crystallization of parental mafic magmas in order to generate a rhyolitic melt with a water content of ~6 wt %. Such a magma should produce a significant cumulate residue. The variable water contents and the absence of CO₂ in Hekla melt inclusions may result from a cooling and degassing body of magma that reached volatile saturation, bled off its CO₂, and was later remelted and remobilized by fresh injections of basalt. This process is consistent with the bulk solidification and partial remelting of basalts at depth.

Interactions between melts with variable densities and incompatible components, such as K₂O and H₂O, would lead to a stratified magma chamber as suggested by the zoned deposits. In the case of H3, the model of *Lange* [1997] yields a density of 2600, 2380, and 2300 g/L for H3 dark top, light top, and base, respectively, which is consistent with a layered magmatic reservoir. In this study, we found only one indication of mixing from a single olivine in H3 dark top, but other studies have reported zonation in plagioclase crystals consistent with magma mixing [Sverrisdottir, 2007]. *Sverrisdottir* [2007] also proposed that a decrease in the modal percentage of olivines in hybrid magmas is due to their remelting in a melt of higher temperature. Our calculations using olivine-melt thermometry [Putirka, 2008] yield a temperature difference of 30°C between rhyolite and dacite and a difference of 100°C between rhyolite and basaltic andesite.

This potential process of solidification and remelting brings into question the saturation state of the newly generated melt. If no CO₂ is present during remelting, then the initial melt may contain water but may be volatile undersaturated. Models of rhyolite generation at Hekla require an additional step of fractional crystallization from dacites [Sigmarsson et al., 1992]. If this is the case, then the increasing water contents in evolved rhyolites (e.g., 1104 and H4 compared to H3) suggest that the initial magmatic liquids generated by remelting may be water undersaturated.

5.4. Magma Storage Depths

Using the most volatile-rich melt inclusions in more evolved compositions, we estimate minimum vapor saturation pressures of 204 MPa for H3, 203 MPa for 1104, 80 MPa for 1845, and 14.5 MPa for 1991 (VolatileCalc [Newman and Lowenstern, 2002; Papale et al., 2006]; SolEx [Witham et al., 2012]). Using a crustal density of 2900 kg m⁻³ [Allen et al., 2002], we calculate a minimum entrapment depth of 7.2 km for H3, 7.1 km for 1104, 3 km for 1845, and 0.5–0.7 km for 1991.

The highest H₂O contents in H3 and the highest H₂O and CO₂ contents in 1104 give a similar depth estimate of ~7 km. This is a minimum value if the magmas were volatile undersaturated. If they are volatile saturated or close to saturation, then the 7 km is a robust estimate. This depth is in agreement with observations of *Kjartansson and Gronvold* [1983], *Linde et al.* [1993], *Sigmundsson et al.* [1992], and *Ofeigsson et al.* [2011] suggesting a magma chamber within the 5–9 km depth range. *Linde et al.* [1993] proposed that the propagation of a dyke immediately before the 1991 was initiated at 4 ± 1 km depth from the roof of the magma chamber centered at a depth of 6.5 km. Our estimates of storage depth for the 1845 and 1991 eruptions are minima due to their volatile-undersaturated nature, indicating that they are stored at depths greater than 0.7–3 km. In this regard, *Soosalu and Einarsson* [2004] discounted the possibility of a reservoir shallower than 4 km depth based on their *S* wave attenuation data. Furthermore, given the lack of hydrothermal manifestations at the surface, a substantial shallow crustal reservoir beneath Hekla appears unlikely [Ilyinskaya et al., 2015].

Observations by *Geirsson et al.* [2012] and a review by *Sturkell et al.* [2013] acknowledge the likelihood of magma storage deeper in the crust at depths >15 km. We cannot discount the possibility that more primitive magmas, such as 1845 and 1991, are stored at these depths in another magma chamber. If the

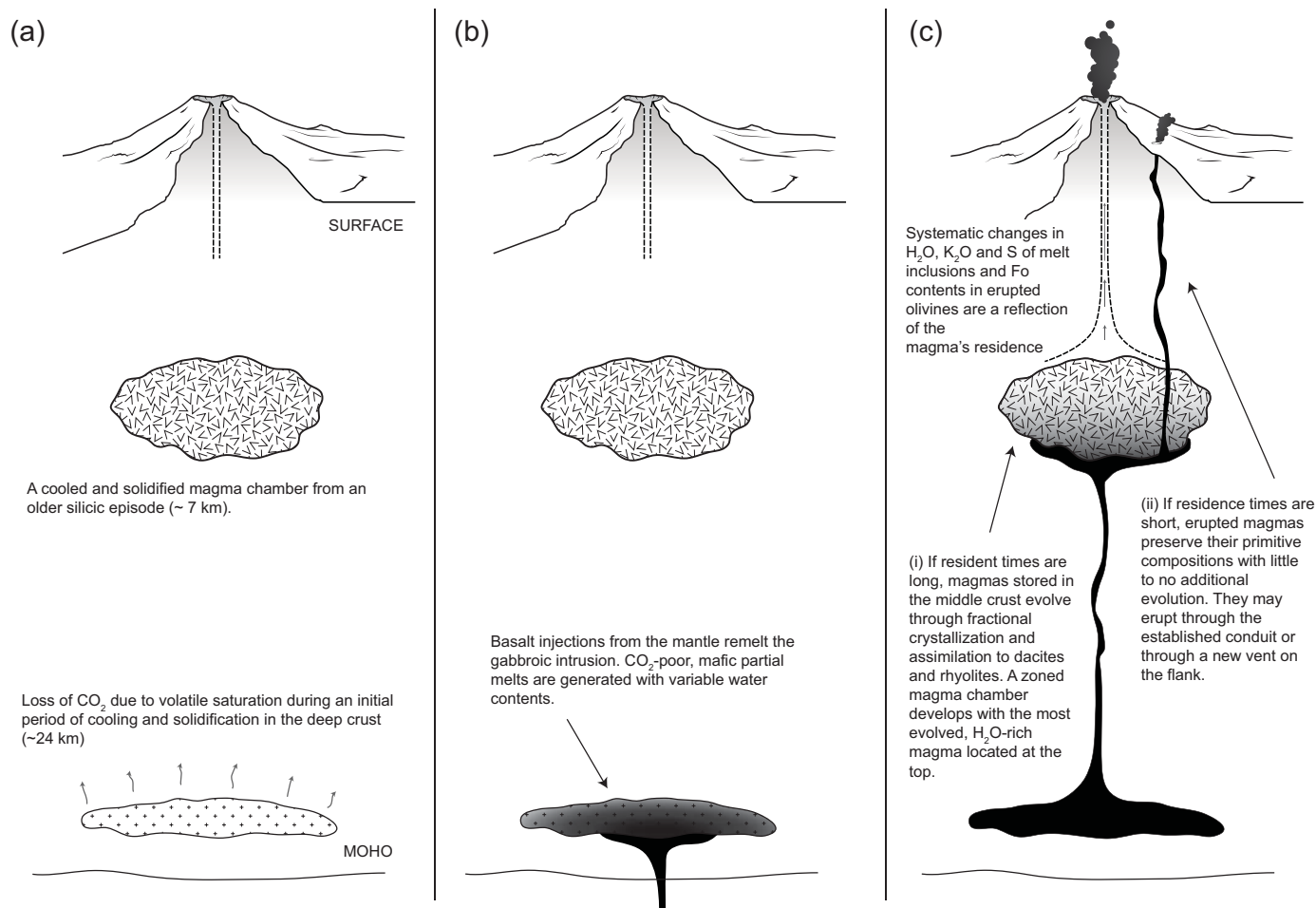


Figure 10. Conceptual model for magmatic and volatile evolution at Hekla. (a) Cooling and solidification of mafic magmas at depth increases the H₂O and CO₂ content of the melt until volatile saturation is reached. At this point, CO₂ is preferentially lost from the system through degassing. Any silicic magmas that remain in the main magma chamber from previous eruptions will also undergo cooling and degassing. (b) New injections of basaltic melt into the magma chamber at depth create partial melts of CO₂-poor mafic magmas. New, volatile-undersaturated melts are produced with variable H₂O contents. (c) These then rise and evolve to dacites and rhyolites through fractional crystallization and assimilation of previous silicic intrusives. A zoned magma chamber forms with the most evolved, volatile-rich rhyolitic magma located at the top. If the system is destabilized, an eruption is triggered. If the volume of erupted material is sufficiently large and most of the magma chamber is emptied (e.g., H3), a zoned deposit is produced. Melt inclusions from these deposits reflect loss of H₂O by synergistic degassing, adding to the variability of H₂O observed in the melt inclusions. *Chekol et al.* [2011] proposed that during shorter repose intervals, injections of mafic magma may bypass such crystallized bodies of magma and erupt with little to no remelting. This is consistent with eruptions of more mafic compositions from vents on the flank of Hekla's edifice.

minimum saturation depth for H3 base and 1104 base is calculated at ~7 km, then the later erupted magmas of H3 and 1104 were likely stored at greater depths. The fact that samples from H3 dark top and 1104 dark top give entrapment depths of ~2.5 km, similar to 1845 and 1991, reinforces the notion that melt inclusions at Hekla are not reliable indicators of storage depths due to potential processes such as synergistic degassing. This implies that less evolved magmas, such as those of 1845 and 1991, may also reside at 7 km or deeper.

The $\delta^{18}\text{O}$ compositions of Hekla magmas suggest they have undergone minimal assimilation of hydrothermally altered crust. In a recent review of silicic, water-rich magma generation in Iceland, *Schattel et al.* [2014] proposed that $\delta^{18}\text{O}$ may be used as a proxy for the storage depths of magmas. Reservoirs that are located in the shallow crust (~1–3 km) are more likely to assimilate oxidized (high $f\text{O}_2$) and hydrothermally altered low- $\delta^{18}\text{O}$ crust (–3 to +1‰), while reservoirs located at greater depths (~6–8 km) are less affected by assimilation of metabasalts, producing magmas with normal crustal $\delta^{18}\text{O}$ signatures (+4 to +6‰) and lower states of oxidation (low $f\text{O}_2$). This model is appropriate and consistent with the petrologic and geophysical character of Hekla.

5.5. Volatile Evolution and the Plumbing Network Beneath Hekla

Eruptive activity at Hekla displays a remarkable range in eruptive styles and products. While the prehistoric period was characterized by large, explosive eruptions of silicic magma, in historic times eruptive products have become more mafic and eruptions smaller. This change in the character of Hekla most likely reflects a periodic reconfiguration of the plumbing network. A trend toward shorter repose intervals over the last 750 years suggests that an efficient conduit system has been established.

Combining the findings of this study with past work on Hekla's deposits and geophysical observations, we propose the following model of magmatic activity (Figure 10). Basalts intrude into the lower crust, remelting previous gabbroic intrusives. The variable water contents and low CO₂/Nb ratios of the melt inclusions are consistent with solidification and subsequent generation of CO₂-poor partial melts. If residence times in the crust are short, the erupted melts are mafic. If residence times are sufficiently long, the new melts can evolve to dacites and rhyolites through additional fractional crystallization and assimilation, ultimately forming zoned magma chambers with variable incompatible components (H₂O and K₂O). This scenario is consistent with the systematic changes observed for forsterite contents in olivine and K₂O, H₂O, and S in melt inclusions across the spectrum of compositions.

Olivine compositions for each of the four eruptions we studied represent a very narrow range in Fo contents, suggesting that the erupted olivines crystallized shortly before eruption or even during eruption as the magma ascended. Hence volatiles trapped within melt inclusions likely represent the volatile state of the magma soon before or during eruption. During magma ascent, syneruptive degassing contributes to the variability of H₂O. Deposits that formed from the explosive, initial phase of the eruption preserve melt inclusions with the highest volatile contents. These melts have likely experienced the least amount of syneruptive degassing due to their rapid ascent [Soosalu and Einarsson, 2004].

Due to the range of volatile contents, only the most volatile-rich melt inclusions within a single deposit are potentially useful indicators of magma storage. According to these melt inclusions, in prehistoric times, the magma chamber may have been located at a depth of ~7 km. But even these data may underestimate the true storage depth or depths of the most silicic magmas at Hekla. If the most water-rich melt inclusions are not at volatile saturation, then the possibility exists that extremely water-rich magmas are stored at mid-crustal levels beneath Hekla. Such magmas should exhibit extreme explosivity upon eruption.

The potentially undersaturated nature of Hekla's less evolved magmas prevents an accurate assessment of storage depths from these compositions. The efficient state of Hekla's plumbing network in historic times may enable the storage and ascent of magmas from deep levels. Deeper storage within a closed system, paired with the undersaturated state of the magma, is consistent with the lack of substantial surface degassing during repose periods in recent years.

6. Conclusions

Hekla volcano is a remarkable natural laboratory for the study of magmatic evolution through time. Our direct measurements of H₂O, CO₂, S, and Cl in melt inclusions from four of Hekla's eruptions shed light on the relationship between repose interval, magmatic evolution, explosivity, and the wide range of volatile contents seen in Icelandic magmas. This data set expands on and complements the current set of volatile data at Hekla volcano and provides an additional set of constraints on the configuration of the plumbing network. Our principal conclusions are as follows:

1. The entire suite of olivine-hosted melt inclusions records a wide range of H₂O contents (0.8–5.67 wt %). Silicic melts (H3 and 1104) have the highest dissolved water contents, followed by intermediate (1845) and mafic liquids (1991) with the lowest amounts of water. The range in water contents within larger, zoned eruptions is the result of syneruptive degassing.
2. This study marks the first instance where CO₂ was detected in Hekla melts. The only eruption with significant CO₂ is 1104 (<10–170 ppm), the most evolved rhyolitic unit. In general, Hekla melts are extremely CO₂ poor, most likely reflecting an early stage of cooling and solidification at depth with concomitant CO₂ degassing.
3. Sulfur concentrations decrease with magmatic evolution, consistent with lower S solubility and increased sulfide precipitation.

4. Melts evolve from basaltic andesite to rhyolite through fractional crystallization, assimilation and partial remelting. Water behaves as an incompatible component and increases in more evolved compositions. The continuous trend of water increases from basalt to rhyolite along with evidence of syneruptive degassing suggests that the large majority of Hekla magmas are volatile undersaturated prior to eruption.
5. The most volatile-rich samples from the first erupted material in H3 and 1104 give minimum depth estimates of ~ 7 km for the upper part of the magma chamber. These depths are in broad agreement with geophysical estimates of storage depths from recent eruptions. We cannot demonstrate or discount the possibility of magma movement and storage at greater depths (10–20 km) due to the likelihood of volatile-undersaturated magmas. Depths we have obtained using volatile saturation pressures at Hekla are minimum estimates.

The generation of water-rich, silicic melts along spreading plate boundaries remains a topic of discussion and debate. In order to better understand the explosive potential of volcanic centers such as Hekla, our understanding of magmatic evolution and storage must improve. Despite comprehensive studies of deformation, seismicity, and magmatic and volatile evolution, the exact configuration of Hekla's plumbing network remains elusive. Recent geothermal exploration at Krafla volcano has demonstrated the difficulty in detecting reservoirs of magma in the shallow crust [Elders *et al.*, 2011], and it poses the question of how many other undetected reservoirs are present beneath Icelandic volcanoes.

References

- Allen, R. M., et al. (2002), Plume-driven plumbing and crustal formation in Iceland, *J. Geophys. Res.*, *107*(B8), doi:10.1029/2001JB000584.
- Baker, D. R., and R. Moretti (2011), Modeling the solubility of sulfur in magmas: A 50-year old geochemical challenge, *Rev. Mineral. Geochem.*, *73*(1), 167–213, doi:10.2138/rmg.2011.73.7.
- Baldrige, W. S., T. R. McGetchin, F. A. Frey, and E. Jarosewich (1973), Magmatic evolution of Hekla, Iceland, *Contrib. Mineral. Petrol.*, *42*(3), 245–258, doi:10.1007/BF00371589.
- Behrens, H., N. Tamic, and F. Holtz (2004), Determination of the molar absorption coefficient for the infrared absorption band of CO₂ in rhyolitic glasses, *Am. Mineral.*, *89*(2-3), 301–306.
- Bindeman, I., A. Gurenko, T. Carley, C. Miller, E. Martin, and O. Sigmarsson (2012), Silicic magma petrogenesis in Iceland by remelting of hydrothermally altered crust based on oxygen isotope diversity and disequilibria between zircon and magma with implications for MORB, *Terra Nova*, *24*(3), 227–232, doi:10.1111/j.1365-3121.2012.01058.x.
- Chokol, T. A., K. Kobayashi, T. Yokoyama, C. Sakaguchi, and E. Nakamura (2011), Timescales of magma differentiation from basalt to andesite beneath Hekla Volcano, Iceland: Constraints from U-series disequilibria in lavas from the last quarter-millennium flows, *Geochim. Cosmochim. Acta*, *75*(1), 256–283, doi:10.1016/j.gca.2010.10.001.
- Cioni, R., L. Civetta, P. Marianelli, N. Metrich, R. Santacroce, and A. Sbrana (1995), Compositional layering and syn-eruptive mixing of a periodically refilled shallow magma chamber: The AD 79 plinian eruption of Vesuvius, *J. Petrol.*, *36*(3), 739–776, doi:10.1093/petrology/36.3.739.
- Costa, F., and B. Singer (2002), Evolution of Holocene dacite and compositionally zoned magma, volcán San Pedro, Southern Volcanic Zone, Chile, *J. Petrol.*, *43*(8), 1571–1593, doi:10.1093/petrology/43.8.1571.
- Devine, J. D., J. E. Gardner, H. P. Brack, G. D. Layne, and M. J. Rutherford (1995), Comparison of microanalytical methods for estimating H₂O contents of silicic volcanic glasses, *Am. Mineral.*, *80*(3-4), 319–328.
- Dugmore, A., G. T. Cook, J. S. Shore, A. Newton, K. J. Edwards, and G. Larsen (1995), Radiocarbon dating tephra layers in Britain and Iceland, *Radiocarbon*, *37*(2), 379–388.
- Elders, W. A., et al. (2011), Origin of a rhyolite that intruded a geothermal well while drilling at the Krafla volcano, Iceland, *Geology*, *39*(3), 231–234, doi:10.1130/g31393.1.
- Erlund, E. J., K. V. Cashman, P. J. Wallace, L. Pioli, M. Rosi, E. Johnson, and H. D. Granados (2010), Compositional evolution of magma from Parícutin Volcano, Mexico: The tephra record, *J. Volcanol. Geotherm. Res.*, *197*(1–4), 167–187, doi:10.1016/j.jvolgeores.2009.09.015.
- Finney, B., S. Turner, C. Hawkesworth, J. Larsen, C. Nye, R. George, I. Bindeman, and J. Eichelberger (2008), Magmatic differentiation at an island-arc caldera: Okmok Volcano, Aleutian Islands, Alaska, *J. Petrol.*, *49*(5), 857–884, doi:10.1093/petrology/egn008.
- Gaetani, G. A., J. A. O'Leary, N. Shimizu, C. E. Bucholz, and M. Newville (2012), Rapid reequilibration of H₂O and oxygen fugacity in olivine-hosted melt inclusions, *Geology*, *40*(10), 915–918, doi:10.1130/g32992.1.
- Geirsson, H., P. LaFemina, T. Árnadóttir, E. Sturkell, F. Sigmundsson, M. Travis, P. Schmidt, B. Lund, S. Hreinsdóttir, and R. Bennett (2012), Volcano deformation at active plate boundaries: Deep magma accumulation at Hekla volcano and plate boundary deformation in south Iceland, *J. Geophys. Res.*, *117*, B11409, doi:10.1029/2012JB009400.
- Gronvold, K., G. Larsen, P. Einarsson, S. Thorarinnsson, and K. Saemundsson (1983), The Hekla eruption 1980–1981, *Bull. Volcanol.*, *46*(4), 349–363, doi:10.1007/BF02597770.
- Gudmundsson, A., et al. (1992), The 1991 eruption of Hekla, Iceland, *Bull. Volcanol.*, *54*(3), 238–246, doi:10.1007/BF00278391.
- Hards, V. L., P. D. Kempton, R. N. Thompson, and P. B. Greenwood (2000), The magmatic evolution of the Snæfell volcanic centre: An example of volcanism during incipient rifting in Iceland, *J. Volcanol. Geotherm. Res.*, *99*(1–4), 97–121, doi:10.1016/S0377-0273(00)00160-8.
- Hartley, M. E., J. Maclennan, M. Edmonds, and T. Thordarson (2014), Reconstructing the deep CO₂ degassing behaviour of large basaltic fissure eruptions, *Earth Planet. Sci. Lett.*, *393*, 120–131, doi:10.1016/j.epsl.2014.02.031.
- Hartley, M. E., D. J. Morgan, J. Maclennan, M. Edmonds, and T. Thordarson (2016), Tracking timescales of short-term precursors to large basaltic fissure eruptions through Fe–Mg diffusion in olivine, *Earth Planet. Sci. Lett.*, *439*, 58–70, doi:10.1016/j.epsl.2016.01.018.

Acknowledgments

The authors would like to thank Karen Harp and Denis Geist for advice and assistance with sampling localities. We thank Patricia Nadeau for her help with sample collection in 2011. We appreciate the assistance provided by Rikke Pederson and Freysteinn Sigmundsson during our fieldwork on Hekla. We are most grateful for water and CO₂ standards provided to us by Jacob Lowenstern, as well as for his discussions regarding FTIR measurements and sample preparation. Lang Shi was instrumental to our measurements with the electron microprobe, and we thank him for his help with the samples. We also thank Kim Berlo, Marc-Antoine Longpré, and Jason Coumans for their thought-provoking discussions and assistance. Reviews by Janne Blichert-Toft, Margaret Hartley, and Tom Sisson substantially improved the paper and are gratefully acknowledged. This research was made possible with funding to G.L. from GEOTOP, MAGNET, and the Department of Earth and Planetary Sciences, McGill University. This study was also funded by Discovery, Accelerator, and Create grants to J.S. from the Natural Sciences and Engineering Research Council of Canada. Supporting data are included as eight tables in a single supporting information file.

- Hattori, K., and K. Muehlenbachs (1982), Oxygen isotope ratios of the Icelandic crust, *J. Geophys. Res.*, *87*(B8), 6559–6565, doi:10.1029/JB087iB08p06559.
- Hauri, E., K. Gronvold, N. Oskarsson, and D. McKenzie (2002), Abundance of carbon in the Icelandic mantle: Constraints from melt inclusions, *Eos Trans. AGU*, *83*(19), Spring Meet. Suppl., Abstract V51D-03.
- Hildreth, W., and C. J. N. Wilson (2007), Compositional zoning of the Bishop Tuff, *J. Petrol.*, *48*(5), 951–999, doi:10.1093/petrology/egm007.
- Humphreys, M. C. S., S. L. Kearns, and J. D. Blundy (2006), SIMS investigation of electron-beam damage to hydrous, rhyolitic glasses: Implications for melt inclusion analysis, *Am. Mineral.*, *91*(4), 667–679, doi:10.2138/am.2006.1936.
- Ilyinskaya, E., et al. (2015), Degassing regime of Hekla volcano 2012–2013, *Geochim. Cosmochim. Acta*, *159*, 80–99, doi:10.1016/j.gca.2015.01.013.
- Jónasson, K. (2007), Silicic volcanism in Iceland: Composition and distribution within the active volcanic zones, *J. Geodyn.*, *43*(1), 101–117, doi:10.1016/j.jog.2006.09.004.
- King, P. L., T. W. Vennemann, J. R. Holloway, R. L. Hervig, J. B. Lowenstern, and J. F. Forneris (2002), Analytical techniques for volatiles: A case study using intermediate (andesitic) glasses, *Am. Mineral.*, *87*(8-9), 1077–1089.
- Kjartansson, E., and K. Gronvold (1983), Location of a magma reservoir beneath Hekla Volcano, Iceland, *Nature*, *301*(5896), 139–141, doi:10.1038/301139a0.
- Kuritani, T., T. Yokoyama, H. Kitagawa, K. Kobayashi, and E. Nakamura (2011), Geochemical evolution of historical lavas from Askja Volcano, Iceland: Implications for mechanisms and timescales of magmatic differentiation, *Geochim. Cosmochim. Acta*, *75*(2), 570–587, doi:10.1016/j.gca.2010.10.009.
- Lacasse, C., H. Sigurdsson, S. N. Carey, H. Jóhannesson, L. E. Thomas, and N. W. Rogers (2007), Bimodal volcanism at the Katla subglacial caldera, Iceland: Insight into the geochemistry and petrogenesis of rhyolitic magmas, *Bull. Volcanol.*, *69*(4), 373–399, doi:10.1007/s00445-006-0082-5.
- Lange, A. R. (1997), A revised model for the density and thermal expansivity of $K_2O-Na_2O-CaO-MgO-Al_2O_3-SiO_2$ liquids from 700 to 1900 K: Extension to crustal magmatic temperatures, *Contrib. Mineral. Petrol.*, *130*(1), 1–11, doi:10.1007/s004100050345.
- Larsen, G., and S. Thorarinnsson (1977), H4 and other acid Hekla tephra layers, *Jökull*, *27*, 28–46.
- Larsen, G., A. Dugmore, and A. Newton (1999), Geochemistry of historical-age silicic tephra in Iceland, *Holocene*, *9*(4), 463–471, doi:10.1191/09596839969624108.
- Linde, A. T., K. Agustsson, I. S. Sacks, and R. Stefansson (1993), Mechanism of the 1991 eruption of Hekla from continuous borehole strain monitoring, *Nature*, *365*(6448), 737–740, doi:10.1038/365737a0.
- Longpré, M.-A., J. Stix, F. Costa, E. Espinoza, and A. Muñoz (2014), Magmatic processes and associated timescales leading to the January 1835 eruption of Cosigüina volcano, Nicaragua, *J. Petrol.*, *55*(6), 1173–1201, doi:10.1093/petrology/egu022.
- Mandeville, C. W., J. D. Webster, M. J. Rutherford, B. E. Taylor, A. Timbal, and K. Faure (2002), Determination of molar absorptivities for infrared absorption bands of H_2O in andesitic glasses, *Am. Mineral.*, *87*(7), 813–821.
- Mangan, M., and T. Sisson (2000), Delayed, disequilibrium degassing in rhyolite magma: Decompression experiments and implications for explosive volcanism, *Earth Planet. Sci. Lett.*, *183*(3–4), 441–455, doi:10.1016/S0012-821X(00)00299-5.
- Martin, E., and O. Sigmarsson (2010), Thirteen million years of silicic magma production in Iceland: Links between petrogenesis and tectonic settings, *Lithos*, *116*(1–2), 129–144, doi:10.1016/j.lithos.2010.01.005.
- Moore, G., A. Chizmeshya, and P. F. McMillan (2000), Calibration of a reflectance FTIR method for determination of dissolved CO_2 concentration in rhyolitic glasses, *Geochim. Cosmochim. Acta*, *64*(20), 3571–3579, doi:10.1016/S0016-7037(00)00447-6.
- Moune, S., O. Sigmarsson, T. Thordarson, and P.-J. Gauthier (2007), Recent volatile evolution in the magmatic system of Hekla volcano, Iceland, *Earth Planet. Sci. Lett.*, *255*(3–4), 373–389, doi:10.1016/j.epsl.2006.12.024.
- Myers, M., P. J. Wallace, and C. J. N. Wilson (2014), Timescales associated with the opening phase of large caldera forming eruptions, Abstract V32A-02 presented at 2014 Fall Meeting, AGU, San Francisco, Calif.
- Neave, D. A., J. MacLennan, T. Thordarson, and M. E. Hartley (2015), The evolution and storage of primitive melts in the Eastern Volcanic Zone of Iceland: The 10 ka Grímsvötn tephra series (i.e. the Saksunarvatn ash), *Contrib. Mineral. Petrol.*, *170*(2), 1–23, doi:10.1007/s00410-015-1170-3.
- Newman, S., and J. B. Lowenstern (2002), VolatileCalc: A silicate melt– H_2O – CO_2 solution model written in Visual Basic for excel, *Comput. Geosci.*, *28*(5), 597–604, doi:10.1016/S0098-3004(01)00081-4.
- Newman, S., E. M. Stolper, and S. Epstein (1986), Measurement of water in rhyolitic glasses; calibration of an infrared spectroscopic technique, *Am. Mineral.*, *71*(11-12), 1527–1541.
- Nicholson, H., M. Condomines, J. G. Fitton, A. E. Fallick, K. Gronvold, and G. Rogers (1991), Geochemical and isotopic evidence for crustal assimilation beneath Krafla, Iceland, *J. Petrol.*, *32*(5), 1005–1020, doi:10.1093/petrology/32.5.1005.
- Ofeigsson, B. G., A. Hooper, F. Sigmundsson, E. Sturkell, and R. Grapenthin (2011), Deep magma storage at Hekla volcano, Iceland, revealed by InSAR time series analysis, *J. Geophys. Res.*, *116*, B05401, doi:10.1029/2010JB007576.
- Ohlhorst, S., H. Behrens, and F. Holtz (2001), Compositional dependence of molar absorptivities of near-infrared OH^- and H_2O bands in rhyolitic to basaltic glasses, *Chem. Geol.*, *174*(1–3), 5–20, doi:10.1016/S0009-2541(00)00303-X.
- Papale, P., R. Moretti, and D. Barbato (2006), The compositional dependence of the saturation surface of $H_2O + CO_2$ fluids in silicate melts, *Chem. Geol.*, *229*(1–3), 78–95, doi:10.1016/j.chemgeo.2006.01.013.
- Portnyagin, M., R. Almeev, S. Matveev, and F. Holtz (2008), Experimental evidence for rapid water exchange between melt inclusions in olivine and host magma, *Earth Planet. Sci. Lett.*, *272*(3–4), 541–552, doi:10.1016/j.epsl.2008.05.020.
- Portnyagin, M., K. Hoernle, S. Storm, N. Mironov, C. van den Bogaard, and R. Botcharnikov (2012), H_2O -rich melt inclusions in fayalitic olivine from Hekla volcano: Implications for phase relationships in silicic systems and driving forces of explosive volcanism on Iceland, *Earth Planet. Sci. Lett.*, *357*–358, 337–346, doi:10.1016/j.epsl.2012.09.047.
- Putirka, K. D. (2008), Thermometers and barometers for volcanic systems, *Rev. Mineral. Geochem.*, *69*(1), 61–120, doi:10.2138/rmg.2008.69.3.
- Roeder, P. L., and R. F. Emslie (1970), Olivine-liquid equilibrium, *Contrib. Mineral. Petrol.*, *29*(4), 275–289, doi:10.1007/BF00371276.
- Rowe, M. C., D. W. Peate, and I. Ukstins Peate (2011), An investigation into the nature of the magmatic plumbing system at Parícutin volcano, Mexico, *J. Petrol.*, *52*(11), 2187–2220, doi:10.1093/petrology/egr044.
- Schattel, N., M. Portnyagin, R. Golowin, K. Hoernle, and I. Bindeman (2014), Contrasting conditions of rift and off-rift silicic magma origin on Iceland, *Geophys. Res. Lett.*, *41*, 5813–5820, doi:10.1002/2014GL060780.
- Sigmarsson, O., M. Condomines, and S. Fourcade (1992), A detailed Th, Sr and O isotope study of Hekla: Differentiation processes in an Icelandic Volcano, *Contrib. Mineral. Petrol.*, *112*(1), 20–34, doi:10.1007/BF00310953.
- Sigmundsson, F., P. Einarsson, and R. Bilham (1992), Magma chamber deflation recorded by the global positioning system: The Hekla 1991 Eruption, *Geophys. Res. Lett.*, *19*(14), 1483–1486, doi:10.1029/92GL01636.

- Silva, S. L. D., and J. A. Wolff (1995), Zoned magma chambers: The influence of magma chamber geometry on sidewall convective fractionation, *J. Volcanol. Geotherm. Res.*, *65*(1–2), 111–118, doi:10.1016/0377-0273(94)00105-P.
- Soosalu, H., and P. Einarsson (2004), Seismic constraints on magma chambers at Hekla and Torfajökull volcanoes, Iceland, *Bull. Volcanol.*, *66*(3), 276–286, doi:10.1007/s00445-003-0310-1.
- Soule, S. A., D. S. Nakata, D. J. Fornari, A. T. Fundis, M. R. Perfit, and M. D. Kurz (2012), CO₂ variability in mid-ocean ridge basalts from syn-emplacment degassing: Constraints on eruption dynamics, *Earth Planet. Sci. Lett.*, *327–328*, 39–49, doi:10.1016/j.epsl.2012.01.034.
- Stix, J., G. Gauthier, and J. N. Ludden (1995), A critical look at quantitative laser-ablation ICP-MS analysis of natural and synthetic glasses, *Can. Mineral.*, *33*(2), 435–444.
- Sturkell, E., K. Ágústsson, A. T. Linde, S. I. Sacks, P. Einarsson, F. Sigmundsson, H. Geirsson, R. Pedersen, P. C. LaFemina, and H. Ólafsson (2013), New insights into volcanic activity from strain and other deformation data for the Hekla 2000 eruption, *J. Volcanol. Geotherm. Res.*, *256*, 78–86, doi:10.1016/j.jvolgeores.2013.02.001.
- Sveinbjörnsdóttir, A. E., M. L. Coleman, and B. W. D. Yardley (1986), Origin and history of hydrothermal fluids of the Reykjanes and Krafla geothermal fields, Iceland, *Contrib. Mineral. Petrol.*, *94*(1), 99–109, doi:10.1007/BF00371231.
- Sverrisdóttir, G. (2007), Hybrid magma generation preceding Plinian silicic eruptions at Hekla, Iceland: Evidence from mineralogy and chemistry of two zoned deposits, *Geol. Mag.*, *144*(04), 643–659, doi:10.1017/S0016756807003470.
- Thorarinsson, S., and G. E. Sigvaldason (1972), The Hekla Eruption of 1970, *Bull. Volcanol.*, *36*(2), 269–288, doi:10.1007/BF02596870.
- Thorarinsson, T. (1967), The eruption of Mt. Hekla 1947–1948. 1—The eruptions of Hekla in historical times, a tephrochronological study, *Soc. Sci. Isl.*, *170*.
- Toplis, M. J. (2005), The thermodynamics of iron and magnesium partitioning between olivine and liquid: Criteria for assessing and predicting equilibrium in natural and experimental systems, *Contrib. Mineral. Petrol.*, *149*(1), 22–39, doi:10.1007/s00410-004-0629-4.
- Toplis, M. J., and M. R. Carroll (1995), An experimental study of the influence of oxygen fugacity on Fe-Ti oxide stability, phase relations, and mineral—melt equilibria in ferro-basaltic systems, *J. Petrol.*, *36*(5), 1137–1170, doi:10.1093/petrology/36.5.1137.
- Von Damm, K. L. (1990), Seafloor hydrothermal activity: Black smoker chemistry and chimneys, *Annu. Rev. Earth Planet. Sci.*, *18*(1), 173–204, doi:10.1146/annurev.ea.18.050190.001133.
- Walker, G. P. L. (1960), Zeolite zones and dike distribution in relation to the structure of the basalts of eastern Iceland, *J. Geol.*, *68*(5), 515–528.
- Wallace, P. J., A. T. Anderson, and A. M. Davis (1995), Quantification of pre-eruptive exsolved gas contents in silicic magmas, *Nature*, *377*(6550), 612–616, doi:10.1038/377612a0.
- Witham, F., J. Blundy, S. C. Kohn, P. Lesne, J. Dixon, S. V. Churakov, and R. Botcharnikov (2012), SolEx: A model for mixed COHSCl-volatile solubilities and exsolved gas compositions in basalt, *Comput. Geosci.*, *45*, 87–97, doi:10.1016/j.cageo.2011.09.021.
- Wood, D. A., I. L. Gibson, and R. N. Thompson (1976), Elemental mobility during zeolite facies metamorphism of the Tertiary basalts of eastern Iceland, *Contrib. Mineral. Petrol.*, *55*(3), 241–254, doi:10.1007/BF00371335.
- Wysoczanski, R., and K. Tani (2006), Spectroscopic FTIR imaging of water species in silicic volcanic glasses and melt inclusions: An example from the Izu-Bonin arc, *J. Volcanol. Geotherm. Res.*, *156*(3–4), 302–314, doi:10.1016/j.jvolgeores.2006.03.024.
- Yamashita, S., T. Kitamura, and M. Kusakabe (1997), Infrared spectroscopy of hydrous glasses of arc magma compositions, *Geochem. J.*, *31*(3), 169–174.
- Zellmer, G., K. Rubin, K. Gronvold, and Z. Juradochichay (2008), On the recent bimodal magmatic processes and their rates in the Torfajökull–Veidivötn area, Iceland, *Earth Planet. Sci. Lett.*, *269*(3–4), 388–398, doi:10.1016/j.epsl.2008.02.026.

Erratum

In the originally published version of this article, the title contained a misspelling. The error has since been corrected, and this version may be considered the authoritative version of record.